EXCITED STATES IN ^{19}F

by

David Lee Sellin

Department of Physics
Duke University

Date: _____

Approved:

_____
Henry W. Newson, Supervisor

_____

_____

_____

_____

A dissertation submitted in partial fulfillment of the requirements for the degree of Doctor of Philosophy in the Department of Physics in the Graduate School of Arts and Sciences of Duke University

1969

ABSTRACT

(Physics)

EXCITED STATES IN ^{19}F

by

David Lee Sellin

Department of Physics
Duke University

Date: _____

Approved:

_____
Henry W. Newson, Supervisor

_____

_____

_____

_____

An abstract of a dissertation submitted in partial fulfillment of the requirements for the degree of Doctor of Philosophy in the Department of Physics in the Graduate School of Arts and Sciences of Duke University

1969

EXCITED STATES IN ^{19}F

by

David Lee Sellin

The $^{18}O(p,p)^{18}O$ and $^{18}O(p,\alpha)^{15}N$ excitation functions were investigated in the energy range $E_p = 1.39$ to 3.20 MeV by simultaneous observation of protons and α-particles at 135°. Only twelve prominent elastic scattering levels were observed at this angle and at 45°, despite the high experimental resolution (less than 400 eV energy spread).

R-matrix expressions for multichannel multilevel cross sections were programmed and used to analyze these data. Three of the resonances were determined to be s-wave and seven d-wave, while only two were found to have odd parity. Spins were assigned to each of these twelve resonances except for one d-wave.

The experimental results were compared with those of a shell model calculation. This model predicts positive parity doorway states in the energy range of the experiment. These states are formed from a 2p-1h model treating the target ^{18}O as the core. It is assumed that these doorway states fragment via couplings with more complex configurations. In this way, each positive parity level observed in the present experiment can be associated with a doorway state. In particular, both the data and the model indicate that the $5/2^+$ level observed at 2.768 MeV may be identified as the analogue of the 3.16 MeV level in ^{19}O; however, isobaric spin impurities are present. No similar fragmentation was observed for the proton interaction with ^{16}O under the same condition.

ACKNOWLEDGMENTS

I would like to thank my advisor, Dr. H. W. Newson, for suggesting the experiment and for his advice and support throughout the work.

I wish to express appreciation to Drs. E. G. Bilpuch, G. A. Keyworth, and G. C. Kyker for significant consultations and contributions. Thanks go to all others who gave of their time. In particular, long hours were spent by Messrs. J. C. Browne, R. A. Hilko, and D. Lindstrom in helping to take the data. Mrs. Joseph Bailey prepared the final drawings.

I am especially grateful to Dr. W. P. Beres for his interest and substantial contributions. Discussions with Drs. L. C. Biedenharn and M. Divadeenam were of value.

Finally, I owe a great debt to my wife, Jacquie, for her encouragement and assistance.

This work was supported in part by the U. S. Atomic Energy Commission, and computations involved in this research were performed at the Triangle Universities Computing Center which is supported in part by the National Science Foundation.

D. L. S.

CONTENTS

LIST OF FIGURES

LIST OF TABLES

EXCITED STATES IN ^{19}F

Chapter I

INTRODUCTION

The compound nucleus ^{19}F has been the subject of considerable experimental activity. However, no consistent analysis has yet been given which both classifies the properties (spins, parities, widths, etc.) of the ^{19}F resonances and interprets them physically in terms of some nuclear model. The high resolution capability of the Duke 3 MeV laboratory provides unique facilities for nuclear structure studies. Specifically, it was decided to investigate the reactions $^{18}O(p,p)^{18}O$, $^{18}O(p,\alpha)^{15}N$, to analyze the data with a multichannel R-matrix code, and to search for analog resonances in this relatively light nucleus. Toward this end, a 2p-1h or doorway shell model interpretation was attempted which would give a physical picture of the nuclear structure underlying these resonances.

Various reactions induced by proton bombardment of ^{18}O have previously been measured and interpreted. Most recently, the $^{18}O(p,n)^{18}F$, $^{18}O(p,p'\gamma)^{18}O$, and $^{18}O(p,\alpha_{1,2}\gamma)^{15}N$ reactions have been analyzed for proton energies between 2.5 and 3.0 MeV (Prosser, Din, and Tolbert, 1967).

A high resolution study of the (p,n) reaction was done by Beard (1964). Yagi et al. (1962) have measured the elastic scattering in the range from E_p = 0.6 to 1.4 MeV; Yagi (1962) has analyzed the data. Carlson et al. (1961) investigated the elastic scattering cross section and the (p,α) reaction for E_p = 0.8 to 3.5 MeV and assigned spins and parities to a few of the many levels observed. Hill and Blair (1956) studied the (p,α) and (p,n) reactions in the same energy range and similarly observed many levels; in a later investigation of the same reactions, Blair and Leigh (1960) determined total cross sections. Mark and Goodman (1956) obtained probable spins for a few levels from angular distributions of the (p,n) reaction.

In the present experiment, the elastic and (p,α) yields have been measured for proton energies from 1.39 to 3.20 MeV at the laboratory angle of 135°. Analysis is restricted to the levels prominent in the elastic yield. Additional elastic data at 45° was taken at energies where the yield is strongly influenced by these prominent levels.

The model used to interpret the data incorporates the ideas of the shell model of Mayer and Jensen (1955) with residual interaction and the concept of doorway states introduced by Block and Feshbach (1963). If an incident proton interacts with a single other target nucleon, the excited state formed may consist of these two excited particles in available single particle states plus a hole left by the "struck" nucleon. Such states are described as two particle one hole (2p-1h) states. The process can continue to form 3p-2h and more complicated states. The residual inter-

action mixes the various possible 2p-1h states. Thus, as described in detail in Chapter III, the states resulting from the model calculation are linear combinations of 2p-1h shell model states.

Chapter II

EXPERIMENT

A. R-Matrix Theory

R-matrix theory as employed here was introduced by Wigner and Eisenbud (1947). The specific expressions used were developed by Lane and Thomas (1958); their notation is used consistently.

Specifically, R-matrix theory assumes the absence of all nuclear processes in which more than two product nuclei are formed. For each pair of nuclei a, an interaction radius a_a is assigned, such that when the radial separation of the two nuclei exceeds a_a, nuclear polarizing forces can be neglected. Thus, for each pair, space is separated into two regions: One, an internal region in which complicated nuclear forces act. Two, an external region in which at most the Coulomb force acts. Nothing more is assumed about the internal region except that the nuclear wavefunction therein can be expanded in terms of a complete set of states, each identified as a nuclear level.

To obtain practical computation of R-matrix cross sections, the computer program MULTI was written. Nuclear potential phase shifts are approximated by hard sphere values; these values are fixed by determining

the interaction radii a_α.

For the present case, phase shifts for the elastic channels are the most critical, since resonance shapes and the magnitude of the cross section generated depend upon them. For protons, the value chosen was $a_\alpha = 5.25$ fm. This value is within 3% of and in between the values of Yagi (1962) and Carlson et al. (1961). In these experiments, the elastic cross section was measured to an accuracy of about ±5%. The relation $a_\alpha = r_o(A_1^{1/3} + A_2^{1/3})$ yields $r_o = 1.45$ fm. These were used to assign the values to the a_α's for the reaction products.

The program is discussed in appendix A; the specific equations programmed are given.

B. Apparatus and Procedure

Most of the experimental apparatus and procedure used are exhaustively described elsewhere. Where this is the case, needless duplication is avoided by presenting only brief descriptions along with the pertinent references.

Development of the apparatus used to take the data has centered on producing nearly monoenergetic beams of protons and neutrons. In this development, two problems have been encountered and effectively dealt with:

One, the energy spread of the incident proton beam from the Van de Graff accelerator has been reduced to about 250 eV. This was accom-

plished by Parks, Newson, and Williamson (1958). The HH^+ beam from the accelerator passes through a 90^o one meter radius electrostatic analyzer to provide energy control and calibration. A signal taken from the image slits of the analyzer provides a correction signal to the energy of the protons. This correction signal can be either directly applied to the target as described by Parks et al. (1958) or used in conjunction with an on line computer as described by Seibel et al. (1967). Thus the slower time-dependent energy variations in the beam used to take the data is thrown away in the process.

Two, the beam spread due to ionization in the target has been reduced to less than 100 eV. This is done by using the "cryostat" developed by Parks et al. (1964) which was later modified by Keyworth et al. (1966) to observe charged particle reactions using solid state detectors. The cryostat is a windowless gas target chamber in which the differential pumping is done cryogenically. Gas escaping from the beam and detector holes in the target chamber is trapped by two concentric cylinders in thermal contact with liquid helium at 4.2^o K. This provides a very thin gas target well localized in the target chamber.

The experiment was started with 0.88 liters of nearly pure ^{18}O ($\geq$ 98%). The equipment and procedure for recovery of this gas to recycle for the next run in described in detail by Beard (1964). This recycling procedure is briefly described in order to explain a modification made on the recovery equipment to provide an improvement on the technique of

Beard.

During each run, the ^{18}O was kept in a reservoir immersed in liquid oxygen; thus the pressure of the ^{18}O gas was assured to be one atmosphere as long as any liquid ^{18}O remained. Under these circumstances, the rate of flow of the gas into the cryostat was held constant by a simple needle valve flow gauge. This constant rate was about 5 cc/min. allowing runs of about 1 1/2 hours before all liquid ^{18}O was exhausted. At this point gas input was halted and the cryostat was isolated from all pumps. Warming up the cryostat released the trapped gas and recovery into a second reservoir was begun. Beard's method of recovery was to trap the gas in the second reservoir by keeping the reservoir immersed in liquid nitrogen. To provide sufficient trapping, this liquid nitrogen had to be pumped on by a mechanical fore pump to reduce its pressure and temperature. It was found that activated charcoal at 77° K, the temperature of liquid nitrogen at atmosphere, provided a far more efficient trap. Accordingly, the second reservoir was replaced by a vertical, 10 1/2" long, 1/2" diameter, stainless steel trap. This was filled about two-thirds full of activated charcoal. Prior to transferring the ^{18}O into the recovery system, this trap was pumped on while being baked for four hours. This removed all gases initially trapped in the charcoal. For recovery, the charcoal was quickly cooled to 77° K by immersing the bottom two-thirds of the trap in liquid nitrogen. After essentially all of the gas was recovered into the charcoal trap, the trap was isolated from the rest of the system and connected to the first or feed

reservoir. By cooling the feed reservoir to 77° K and warming the trap to less than 100° C, 98% of the gas passed back into the feed reservoir, ready for the next run. The remaining 2% of the gas was, of course, not lost but merely remained in the trap during the next run.

The loss of gas per cycle (0.2%) was determined, after many cycles, by measuring the pressure in the feed reservoir at room temperature. Since this pressure never increased, any contamination of the gas by air was gradual and slight. Much of the observed structure was later rechecked at least once and, in all such cases, proved reproducible within the statistical error.

The charged particle cryostat and the electronics used are described more fully by Keyworth (1968). The cryostat provided only a single solid state detector at the fixed angle of 135°. A typical detector spectrum, after linear amplification and biasing to remove low energy noise, is shown in Figure 1. These multichannel spectra were monitored continuously during data taking and used to set "windows" for two single channel analyzers, one including only the p_0 peak, the other only the α_0 peak. The output of each single channel was counter at a fixed energy for a fixed charge as measured by a beam integrator.

The yield curve was taken in 500 eV proton energy steps. Preliminary runs indicated that, in taking smaller steps, too much of the short running time was spent changing the proton energy. Counting times of 30 seconds per point allowed accumulation of 1500 to 2000 counts for the flat

Figure 1. A Typical Detector Spectrum. This spectrum was taken with a 100-channel pulse-height analyzer. The α-particle peak is expanded in the insert. This spectrum was accumulated while data was taken, point by point, over a 15 keV energy range with the average incident proton energy equal to 1.74 MeV.

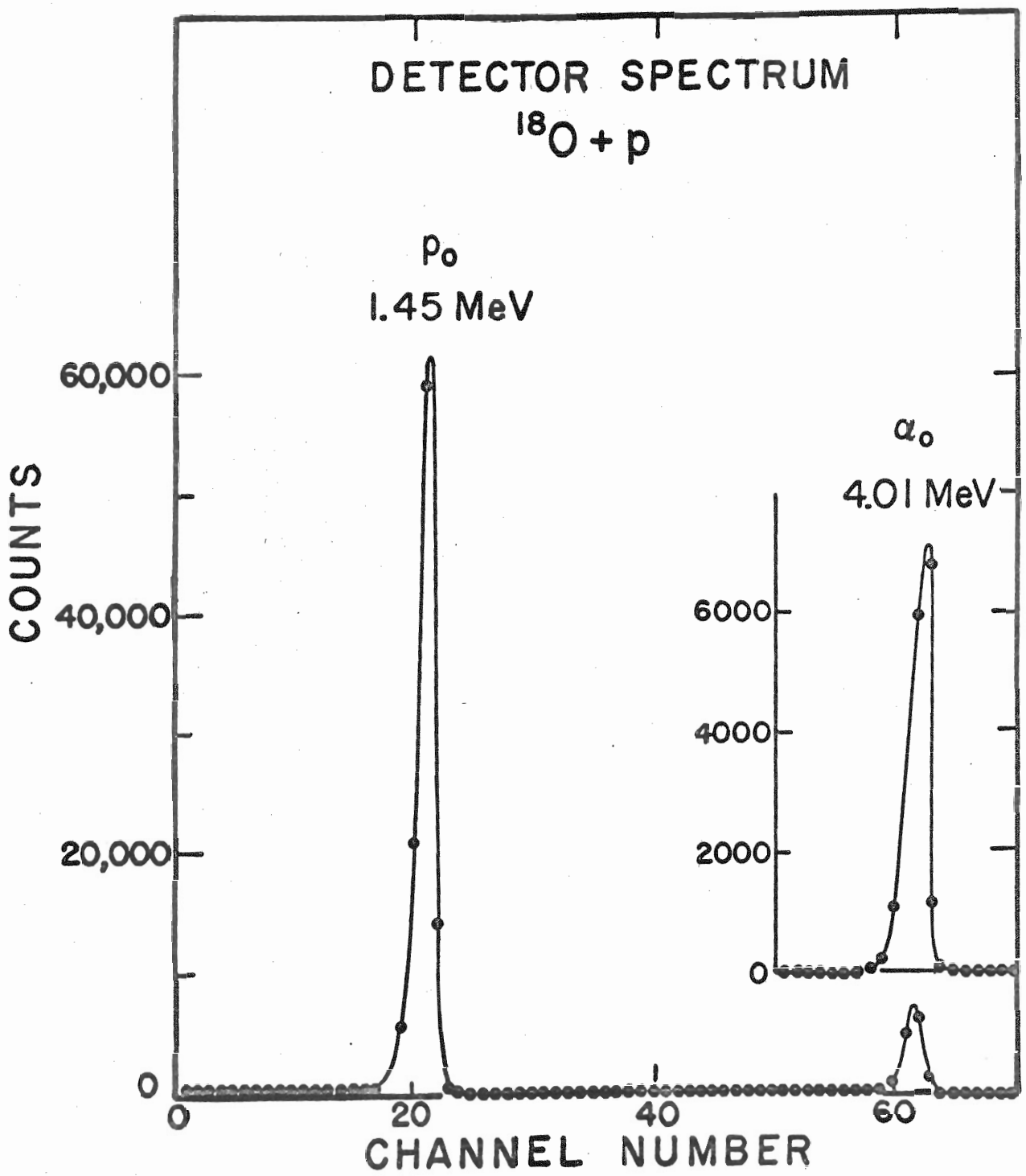
DETECTOR SPECTRUM
$^{18}O + p$
p_o
1.45 MeV
α_o
4.01 MeV
COUNTS
60,000
40,000
20,000
0
6000
4000
2000
0
0
20
40
60
CHANNEL NUMBER

portions of the proton yield. Typical runs covered 40 keV of proton energy.

Above threshold, the $^{18}O(p,n)^{18}F$ yield was monitored with the 20^{o} neutron collimator. However, due to the construction of the cryostat, the neutrons were scattered by nearly an inch of copper and brass before detection; this was found to distort the observed structure, but the stronger (p,n) levels observed by Beard (1964) could be identified.

After the entire yield curve was taken at 135^{o}, the cryostat was rotated 180^{o} to place the detection angle at 45^{o}. Preliminary calculations indicated that those levels prominent in the elastic yield at 135^{o} would also be detectable in the elastic yield at 45^{o}, and that the shapes of these levels would immediately discriminate d-wave resonances from f-wave resonances. These resonant shapes were observed by using the method of data acquisition described by Seibel et al. (1967). In this method, the energy of the accelerator is modulated allowing up to 20 keV of data to be taken at one time.

C. R-Matrix Analysis and Results

The $^{18}O(p,p)^{18}O$ and $^{18}O(p,\alpha)^{15}N$ excitation functions were measured simultaneously at incident proton energies which varied from 1.39 to 3.20 MeV; the elastic protons and α-particles were detected at 135^{o} (Figures 2 and 3). The 55 data runs comprising the energy span were overlapped and normalized to the calculated elastic scattering cross section

Figure 2. The $^{18}O(p,p)^{18}O$ and $^{18}O(p,\alpha)^{15}N$ Data. Except on narrow resonances, every point plotted is the sum of four data points taken.

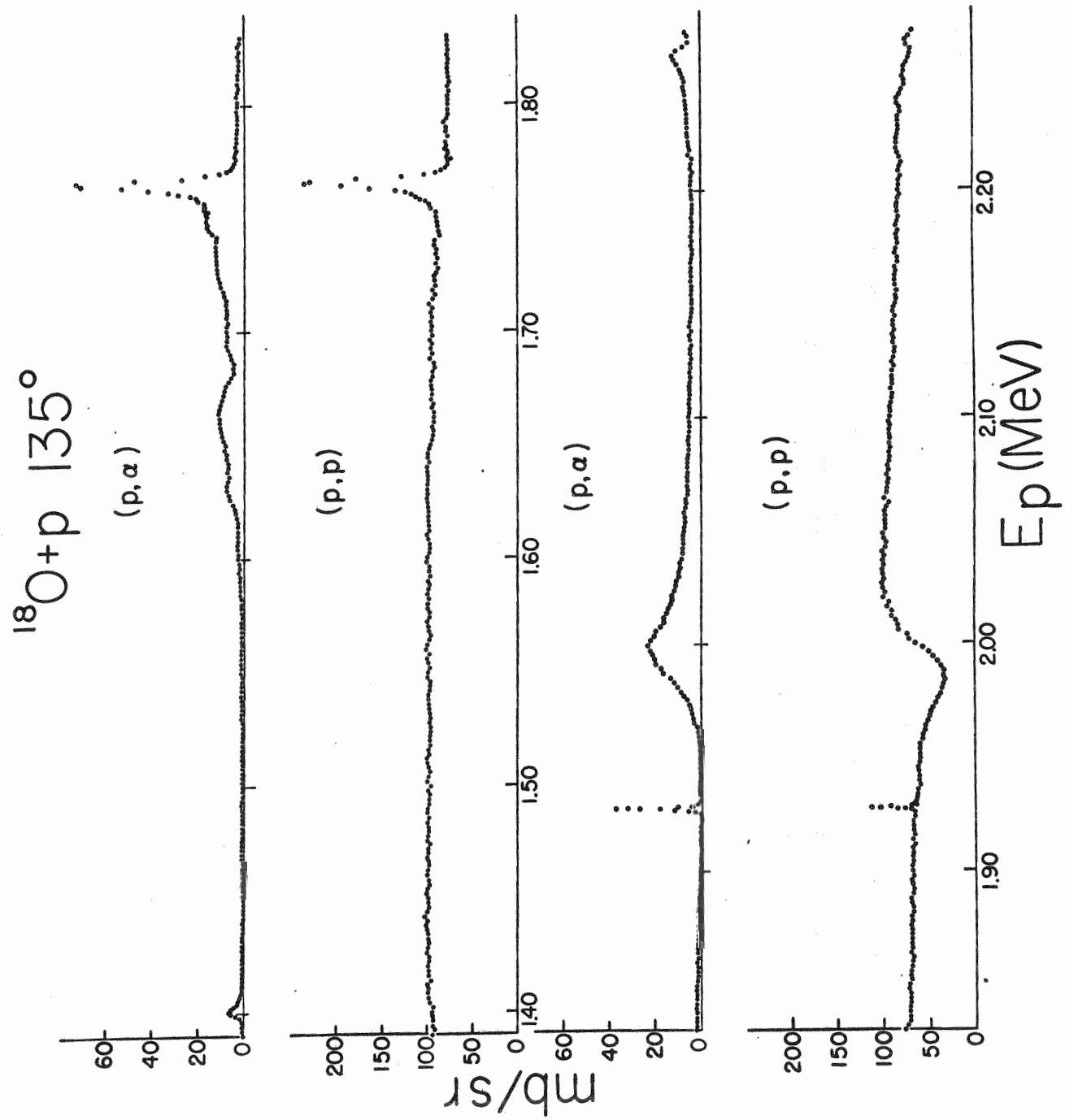
$^{18}O+p$ 135°
(p,α)
(p,p)
(p,α)
(p,p)
mb/sr
Ep (MeV)
60
40
20
0
200
150
100
50
0
1.40
1.50
1.60
1.70
1.80
1.90
2.00
2.10
2.20

Figure 3. Continuation of the (p, p) and (p, α) Data.

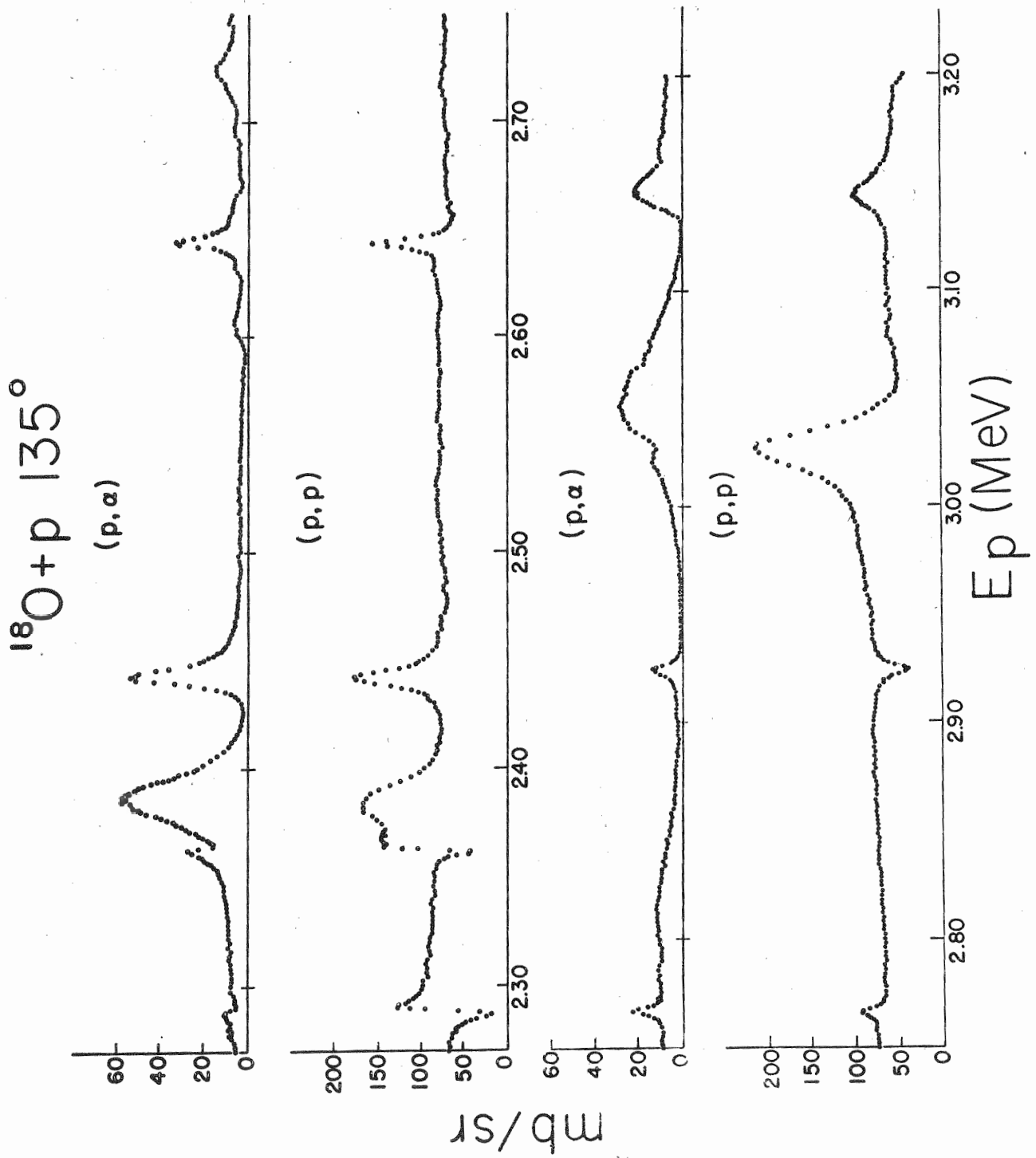
$^{18}O+p$ 135°
(p,α)
(p,p)
(p,α)
(p,p)
mb/sr
Ep (MeV)
60
40
20
0
200
150
100
50
0
2.30
2.40
2.50
2.60
2.70
2.80
2.90
3.00
3.10
3.20

which was obtained by fitting the observed resonant shapes.

The decay modes for the compound nucleus ^{19}F are given in Figure 4 (Lauritsen and Selove, 1962).

Apparently unique results could be obtained only for the twelve levels prominent in the elastic yield. The resonant parameters are given in Table 1; the data is compared to corresponding calculated curves in Figures 5 through 8.

Many difficulties were encountered in obtaining these parameters and establishing their uniqueness. In the computer program MULTI, all parameters are varied manually, with rapid comparison between data and calculation provided by line printer plots. The elastic scattering data at both angles is discussed in the following paragraph.

The resonant shapes are strongly dependent upon the ℓ -values of the levels. Except for the very small probability that $\ell \geq 5$, the values in Table 1 are reliable. For $\ell = 0$ (the 2.001, 2.289, and 2.363 MeV levels), $J^{\pi} = 1/2^{+}$. For $\ell \neq 0$, alternate curves were generated for the two possible values of $J = \ell \pm 1/2$. Level-level interference was found to make the choice decisive for the 2.387 and 2.443 MeV levels and even for the 2.925 and 3.029 MeV levels which are of different spin and parity. For the stronger single levels at 1.766 and 2.644 MeV, the assigned spins fit the 135° data better. Figure 9 compares the two choices for the 2.644 MeV level. For the weaker level at 2.768 MeV ($\Gamma_p/\Gamma = 0.17$), no spin assignment is possible from these data; the assignment shown in the table

Figure 4. The Decay Modes of ^{19}F. Decay to either the first or second excited states of ^{15}N is indicated by $\alpha_{1,2}$. The information was taken from Lauritsen and Selove (1962).

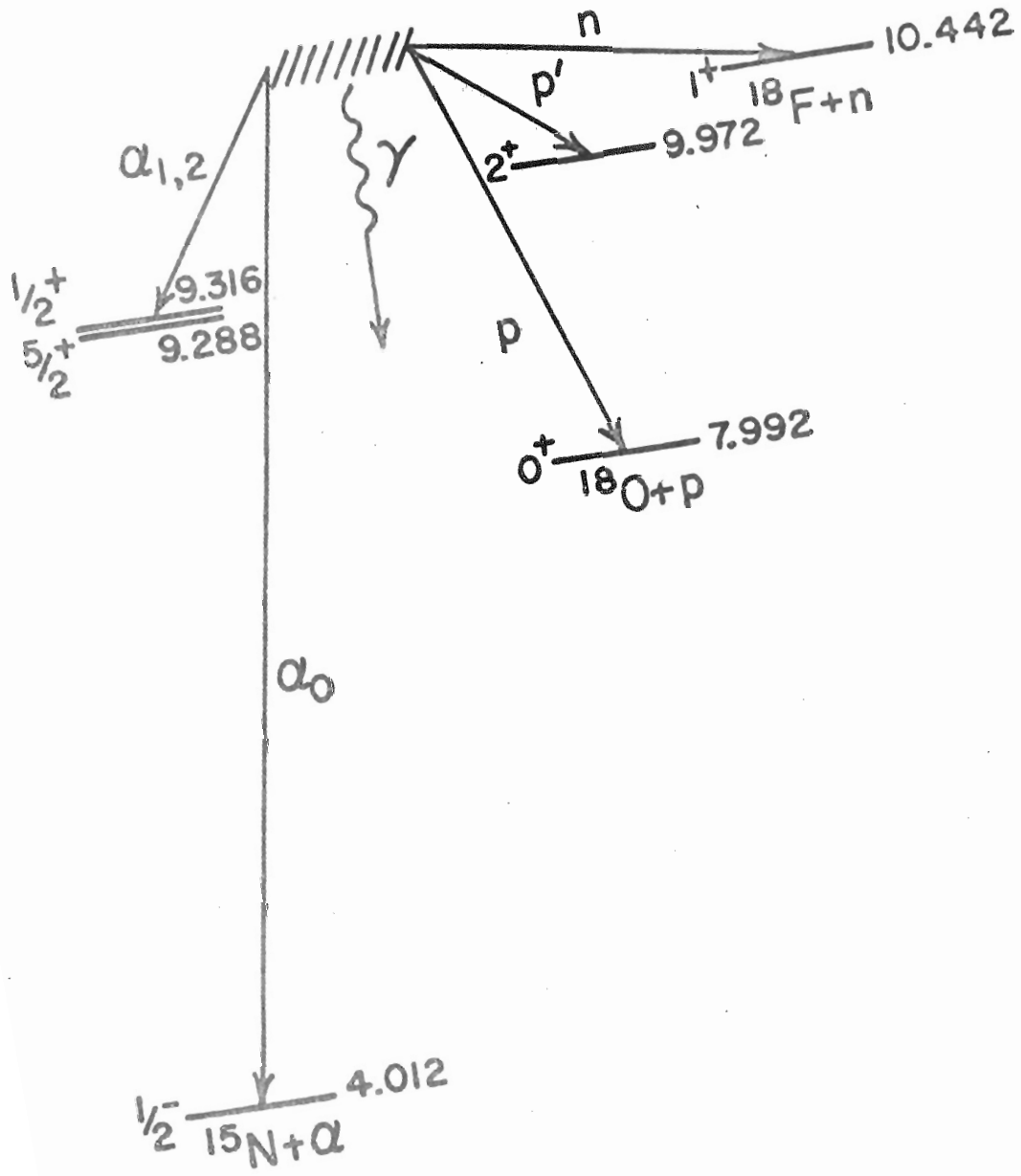
n
10.442
1+
18F+n
p'
9.972
2+
γ
α1,2
1/2+
9.316
9.288
5/2+
p
7.992
0+
18O+p
α0
4.012
1/2-
15N+α
1/2+
0.0
19F

Figure 5. Computer Fitted Cross Section Curves. The parameters were varied by trial and error to fit the observed resonant shapes. Effects due to many more levels are evident; these levels were not included (see text).

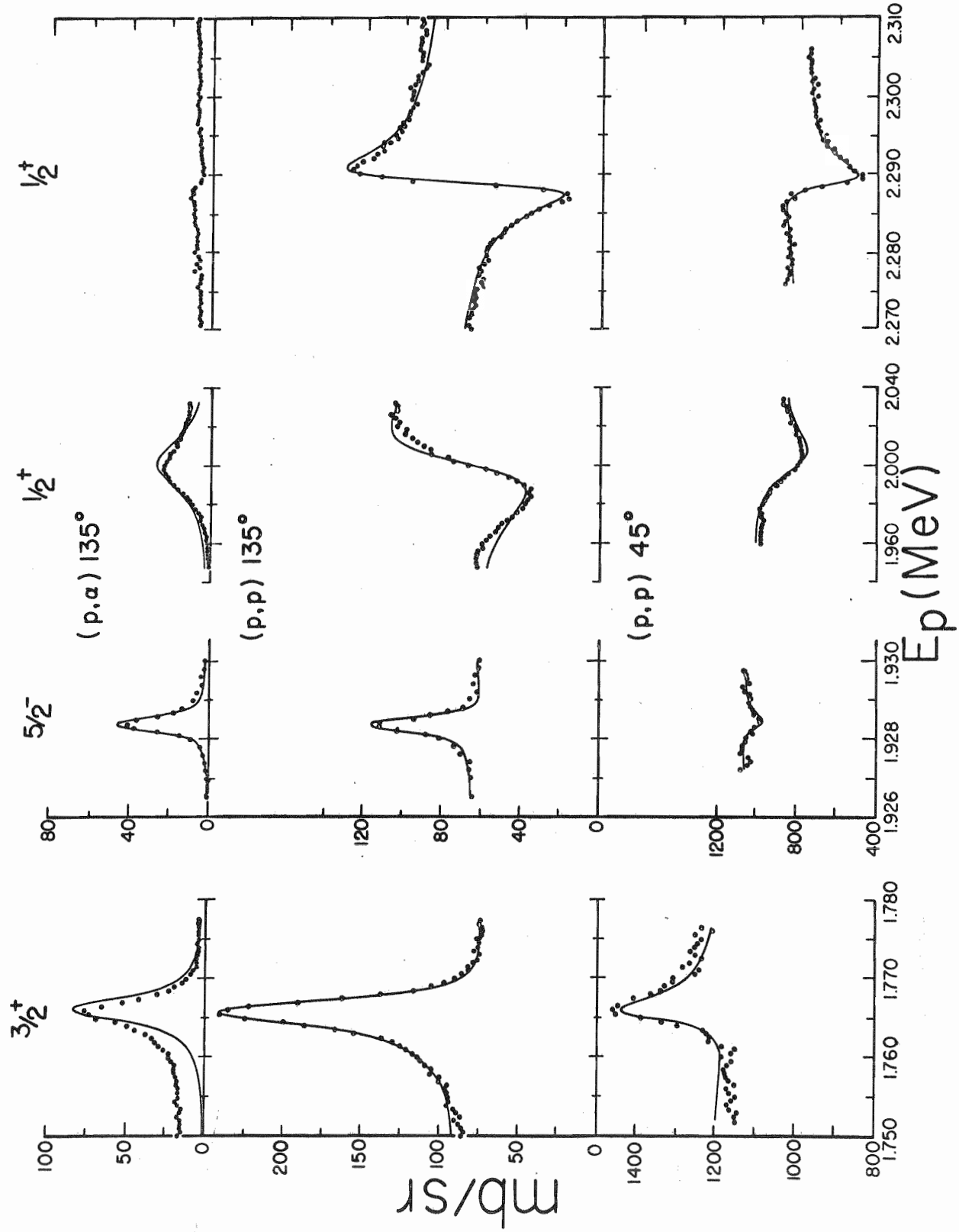
3/2+
5/2−
1/2+
1/2+
(p,α) 135°
(p,p) 135°
(p,p) 45°
mb/sr
Ep (MeV)
100
50
0
200
150
100
50
0
1400
1200
1000
800
80
40
0
120
80
40
0
1200
800
400
1.750
1.760
1.770
1.780
1.926
1.928
1.930
1.960
2.000
2.040
2.270
2.280
2.290
2.300
2.310

Figure 6. Continuation of the Computer Fitted Cross Section Curves.

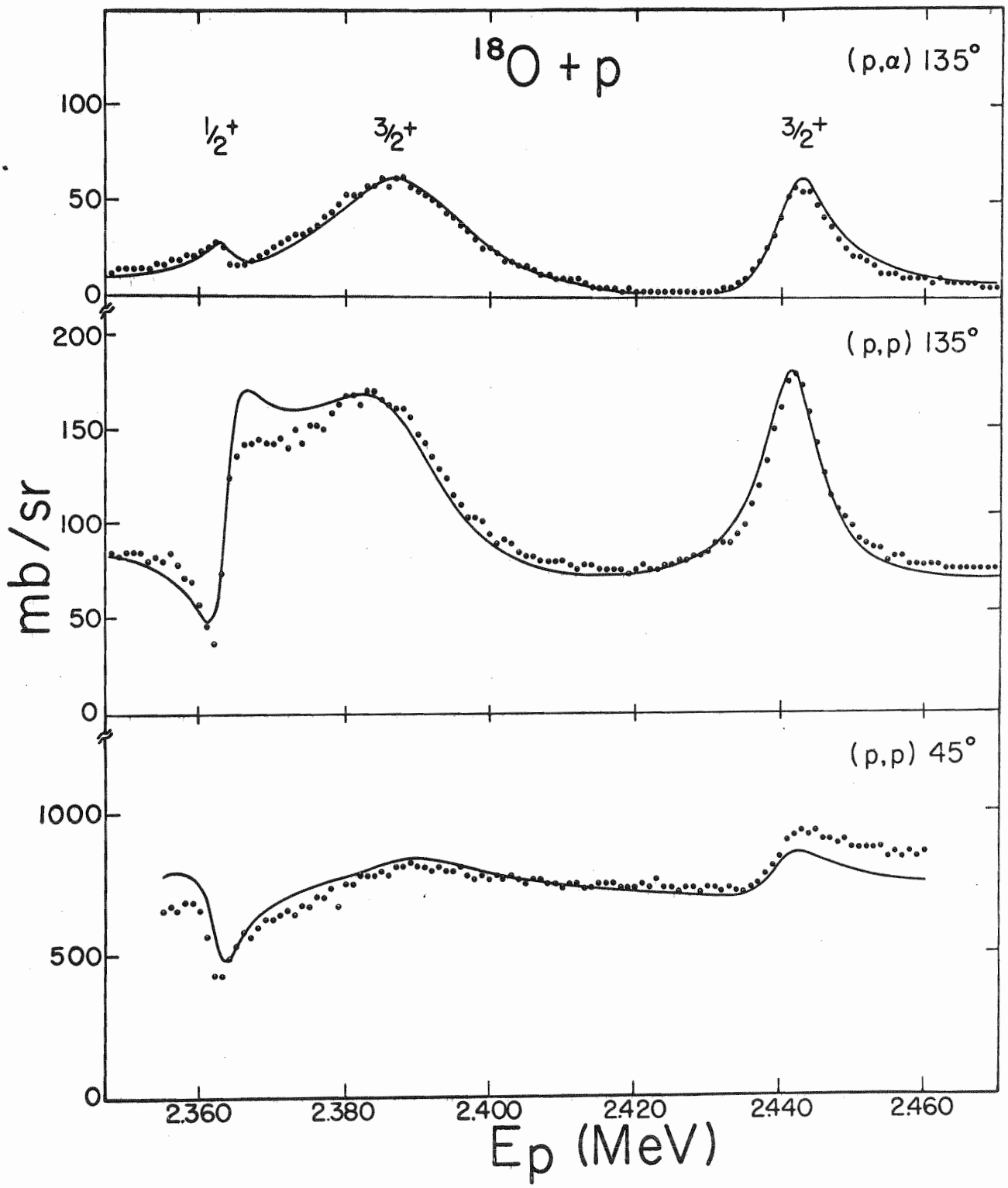
$^{18}O + p$
(p,α) 135°
1/2+
3/2+
3/2+
100
50
0
200
150
100
50
0
(p,p) 135°
mb/sr
1000
500
0
(p,p) 45°
2.360
2.380
2.400
2.420
2.440
2.460
Ep (MeV)

Figure 7. Continuation of the Computer Fitted Cross Section Curves.

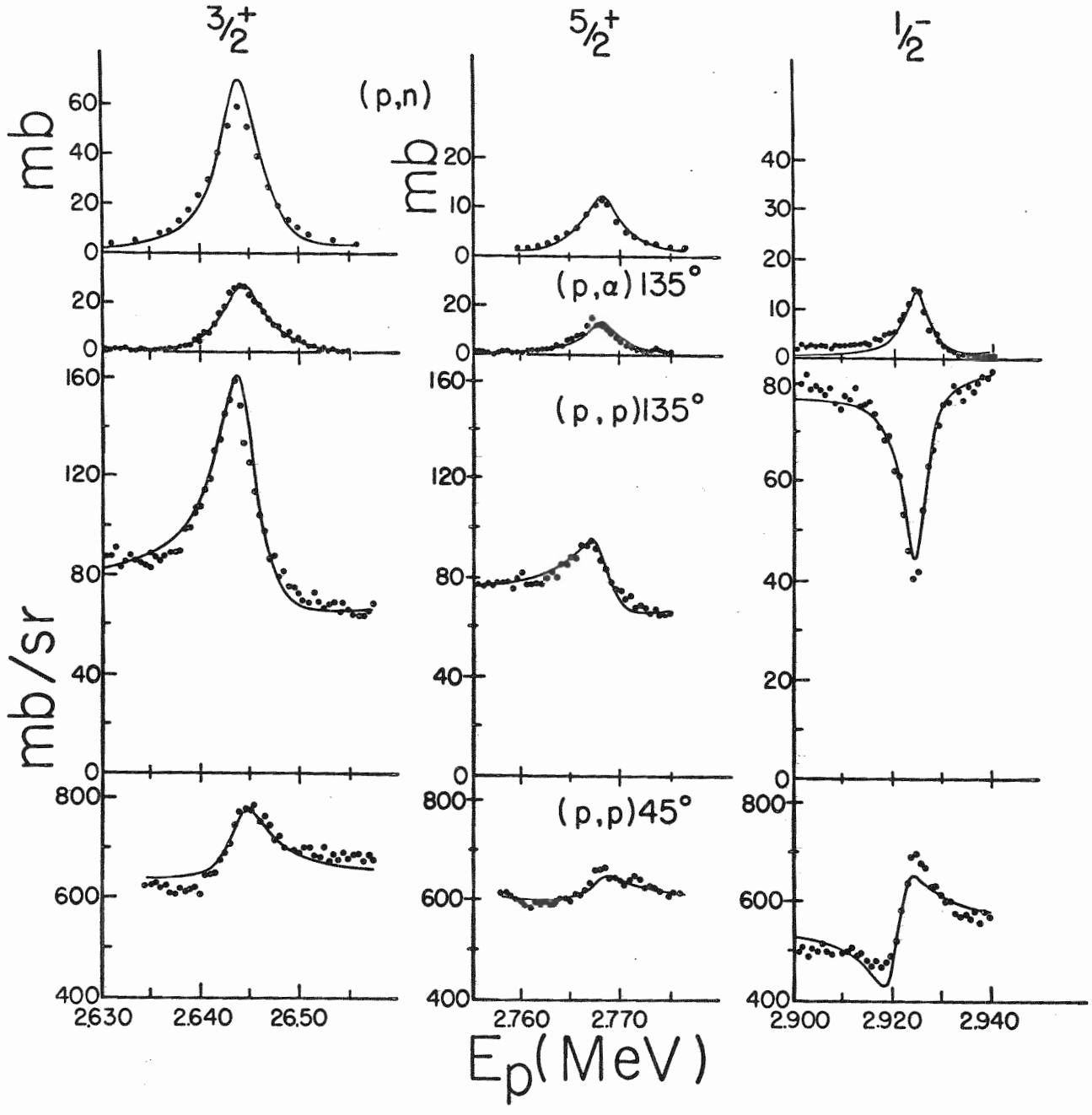
3/2+
5/2+
1/2-
(p,n)
mb
mb
(p,α)135°
(p,p)135°
(p,p)45°
mb/sr
Ep(MeV)
2.630
2.640
26.50
2.760
2.770
2.900
2.920
2.940

Figure 8. Continuation of the Computer Fitted Cross Section Curves. The curves shown for the 3.148 MeV level are for $J = 5/2$ and include interference with the 3.029 MeV level. The solid and broken lines were generated for identical resonant parameters, except the relative sign of two reduced width amplitudes was changed. Neither curve fits the data very well.

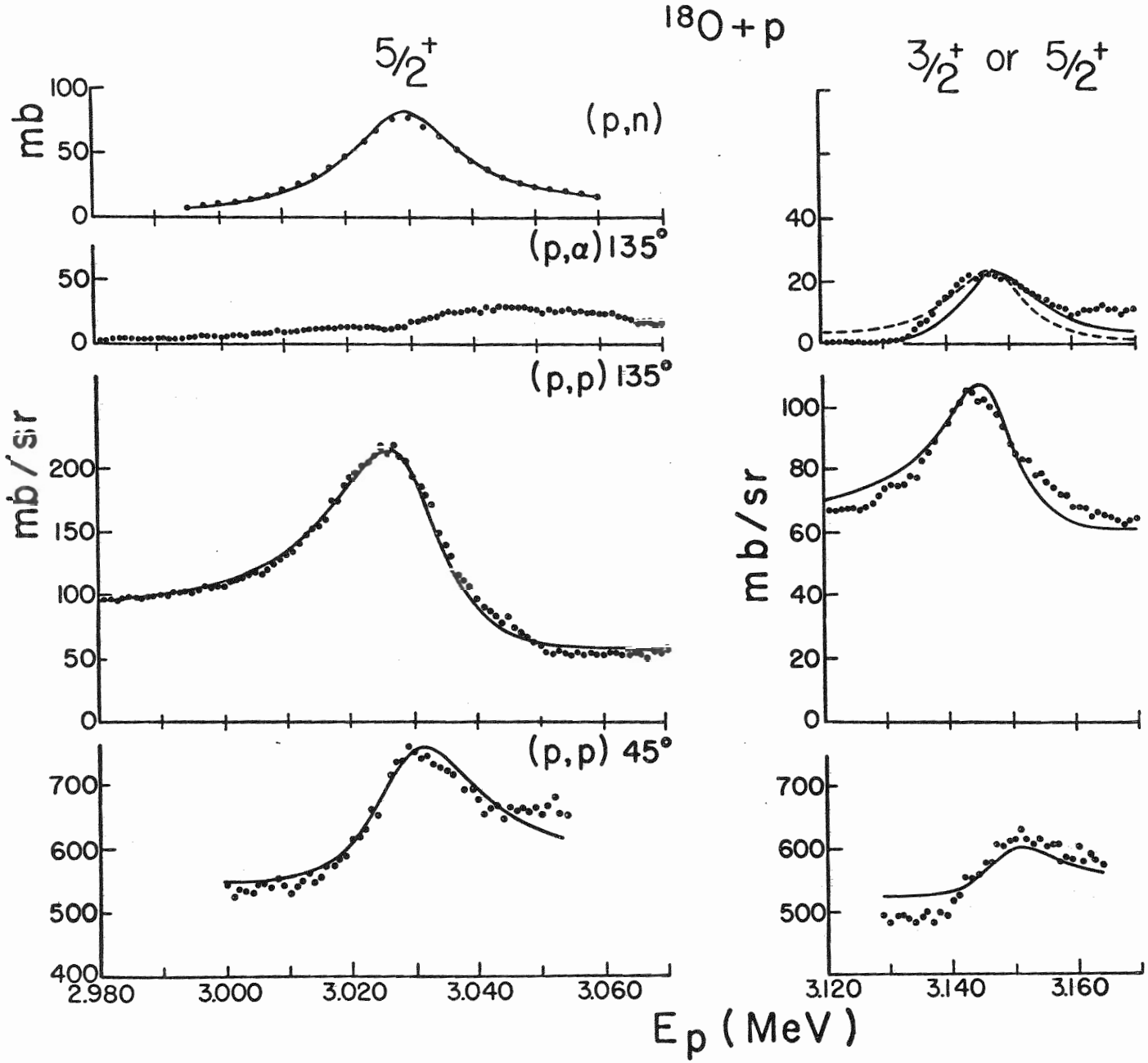
$^{18}O + p$
$5/2^+$
$3/2^+$ or $5/2^+$
(p,n)
(p,α) 135°
(p,p) 135°
(p,p) 45°
mb
mb/sr
100
50
0
40
20
80
60
200
150
700
600
500
400
2.980
3.000
3.020
3.040
3.060
3.120
3.140
3.160
E_p (MeV)

Figure 9. Comparison of Spin Assignments for the 2.644 MeV Resonance. Error bars indicate the statistical error. Fitting both the experimental peak and the off-resonant cross section (indicated by the arrows) determined the listed parameters. As is clearly seen, the $5/2^+$ assignment does not fit the remaining points as well as the $3/2^+$ choice.

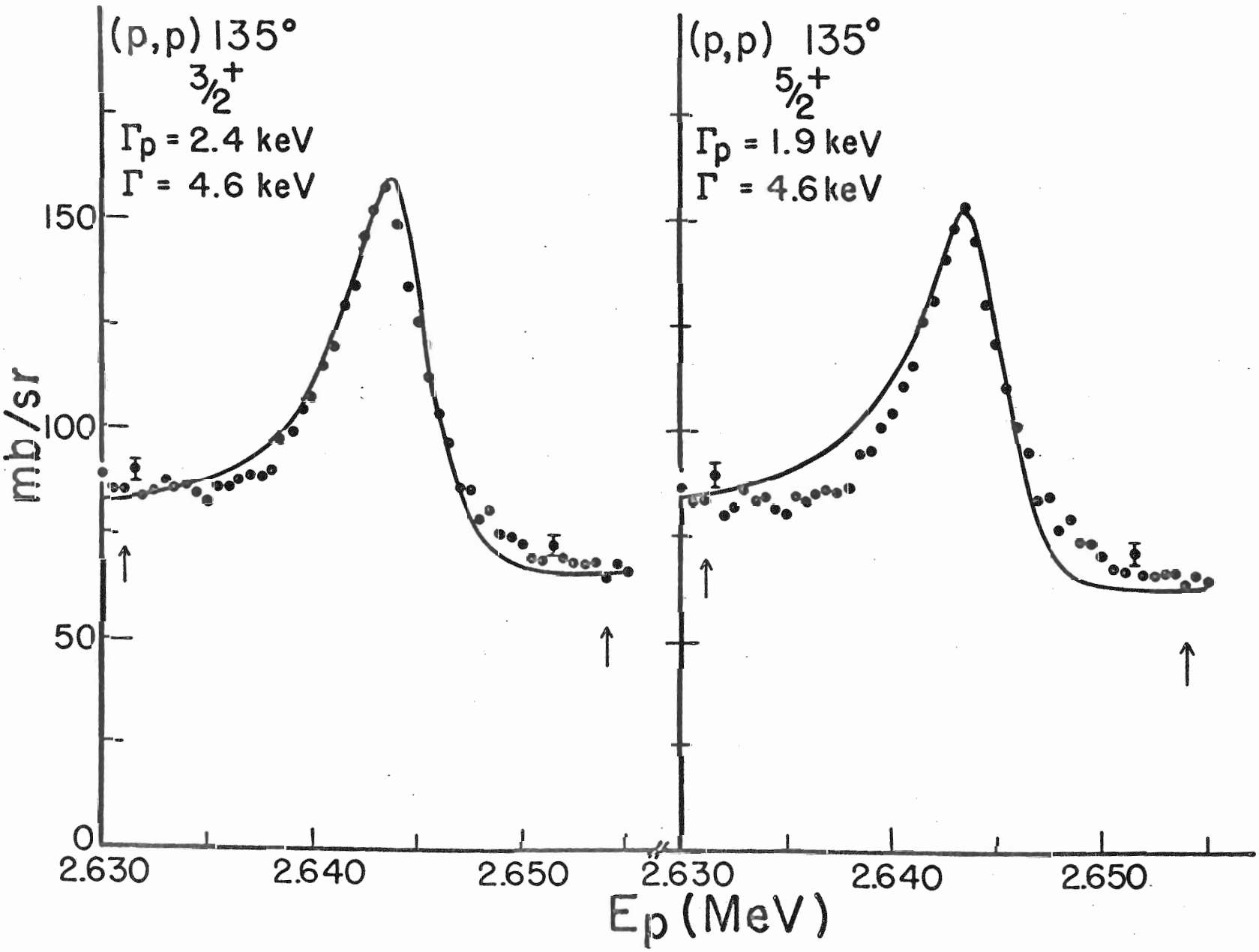
(p,p) 135°
3/2+
Γp = 2.4 keV
Γ = 4.6 keV
(p,p) 135°
5/2+
Γp = 1.9 keV
Γ = 4.6 keV
mb/sr
150
100
50
0
2.630
2.640
2.650
2.630
2.640
2.650
Ep (MeV)

Table 1. Resonant Parameters

E_p (keV)	ℓ	J^π	Γ (keV)	Γ_p (keV)	Γ_α (keV)	Γ_n(estimated) (keV)
1766	2	$3/2^+$	3.6	2.1	1.5	0
1928	3	$5/2^-$	0.165	0.09	0.075	0
		$(7/2)^-$	0.150	0.085	0.065	0
2001 ± 4	0	$1/2^+$	31	12	19	0
2289	0	$1/2^+$	3.3	2.3	(1.0)	0
2363	0	$1/2^+$	4.5	2.8	1.7	0
2387	2	$3/2^+$	24	11	13	0
2443	2	$3/2^+$	9.7	5.2	4.5	0
2644	2	$3/2^+$	4.6	2.4	(1.0)	0.3
2768	2	$5/2^+$	4.0	0.7	(1.1)	0.1
2925	1	$1/2^-$	5.7	4.5	1.2	≈ 0
3029 ± 4	2	$5/2^+$	19.5	13.0	?	0.8
3148 ± 4	2	$(3/2)^+$	(14)	(5)	(4.5)	?
		$(5/2)^+$	(14)	(4)	(4.5)	?

is due to Prosser et al. (1967). Due to possible interference from levels beyond the energy range of the experiment, no unique spin assignment to the 3.148 MeV level is attempted.

Except for one at 1.928 MeV, the levels discussed have widths many times any reasonable estimate of energy resolution. Strong γ-decay was attributed to this level by Carlson et al. (1961). Attempts to fit our α-particle peak height and the elastic scattering data with a Gaussian resolution smear lead to various possibilities which are summarized in Table 2, where Δ is the full width at half maximum of the energy resolution smear and Γ_γ is the proton capture width. As indicated, no curves generated for $J = 7/2$ fit the data well unless $\Delta = 400$ eV, requiring $\Gamma_\gamma = 0$. The results are in reasonable agreement with a spin of 5/2 and a small proton capture width for values of Δ somewhat smaller than 350 eV. Values are given in Table 1 for both spins under the assumption that the proton capture width is negligible; however, the available information indicates that this assumption could possibly be slightly in error for this case. While the 5/2 assignment is favored, the 7/2 possibility is not totally ruled out. Beard (1964) obtained an estimate of Δ which he found to be fairly accurate under similar experimental conditions; the estimate yields $\Delta = 320$ eV at this energy.

For the remaining levels below neutron threshold (2.58 MeV), curves generated for $\Gamma = \Gamma_p + \Gamma_\alpha$ provide reasonable agreement with the stronger α-particle peaks only for the spins assigned in Table 1; these assignments are considered to be unique. The spins and parities of the

Table 2. The 1.928 MeV Level

J^{π}	Γ (eV)	Γ_p (eV)	Γ_α (eV)	Γ_γ (eV)	Δ (eV)
$5/2^-$	310	130	100	80	250
$5/2^-$	165	90	75	0	350
$7/2^-$	150	85	65	0	400

1.766 and 2.001 MeV levels agree with those previously assigned by Carlson et al. (1961).

The remaining levels lie above neutron threshold. In addition, particle decay through the p' and the (unresolved) $\alpha_{1,2}$ channels has been observed by Prosser et al. (1967) above 2.5 MeV and, at higher energies, by Carlson et al. (1961). Attempted fits to the elastic data alone were used to provide spin assignments to the 2.644, 2.925, and 3.029 MeV levels. The same criteria found reliable for the lower energy levels were applied. However, the simplifying assumption that $\Gamma = \Gamma_p + \Gamma_\alpha$ is clearly inaccurate, and the large number of alternative reaction channels introduces a correspondingly large number of partial widths into the calculation. Fortunately, the shape of the 2.644 MeV single level is independent of how these partial widths are assigned, while the level-level interference between the 2.925 and 3.029 MeV levels was found to be governed by the dominant proton partial widths. The values entered in Table 1 are based upon these results. In general, however, the encountered complexity could make it difficult to assign unique spins and parities. Comparison with other experiments is presented in Table 3; values labeled probable or tentative are enclosed in parentheses. As indicated, these assignments agree better with those of Prosser et al. (1967), than with those of Mark and Goodman (1956). Prosser et al. have taken an angular distribution of the $(p,p'\gamma)$ yield at 2.926 MeV. The observed anisotropy is the basis of their $J \geq 5/2$ assignment to the relatively weak resonance they observe at this energy. They

Table 3. Comparison of Spin Assignments and Energies

Present work			Prosser et al.		Mark and Goodman		Beard
E_p (keV)	ℓ	J^π	E_p (keV)	J^π	E_p (keV)	J	E_p (keV)
2644	2	$3/2^+$	2645	(3/2)	2657	-	2643
2768	2	$(3/2,5/2)^+$	2769	$5/2^{(+)}$	2778	-	2767
2925	1	$1/2^-$	2926	($\geq$5/2)	-	-	-
3029	2	$5/2^+$	(3029)	-	3045	($\geq$ 3/2)	3025
3148	2	$(3/2,5/2)^+$	-	-	-	-	3145
-	-	-	-	-	3170	(1/2 ?)	3163

indicate that this assignment is tentative because another source is contributing to the yield and could be the cause of the small anisotropy. Analysis of the present experiment suggest that the 3.029 MeV d-wave resonance is this source and that their assignment should apply to this resonance, not to the 2.925 MeV p-wave resonance.

With few exceptions, the (p, α) yield is not "resolved". The yield appears to be the result of overlapping levels. These levels could have been included in the attempted fits on the basis of guesswork; but even if a particular combination of levels led to nearly perfect agreement, its uniqueness would be difficult to substantiate. Where analysis of the elastic yield provides reasonable interpretation of the (p, α) data, the curves are shown. For the 2.644 and 2.768 MeV levels, Γ_α was estimated by subtracting the α-particle yield from other sources and fitting the remaining peak heights.

Some of the α-particle peaks appear shifted from the energies of the corresponding proton fits (e.g. the 1.766 MeV level). That level-level interference can produce such shifts is demonstrated in the "fit" to the 3.148 MeV level (Figure 8). The curves are shown for $J = 5/2$ and include interference with the 3.029 MeV level. The solid and broken lines were generated for identical resonance parameters, except the relative sign of two reduced width amplitudes was changed. A detailed discussion of the various possibilities is presented in Lane and Thomas (1958).

The 2.644, 2.768, and 3.029 MeV levels appear as relatively well isolated single levels in Beard's measurement of the yield from the

$^{18}O(p,n)^{18}F$ total cross section. Data points were taken from the smooth curve drawn through his data points and thus represent an average of these points. For the 2.644 MeV level, experimental background only was subtracted. For the remaining levels, additional constant background, presumably due to distant levels, was subtracted. Single level shapes did not fit the 3.029 MeV level very well. To approximate the effects of many distant levels, an additional level was included in the fit (E_p = 3.085 MeV, Γ_n = 5 keV, Γ = 19 keV, $J^\pi = 3/2^+$). As discussed above, similar treatment elsewhere was avoided.

Absolute energy calibration was obtained by measurement of the $^7Li(p,n)^7Be$ threshold at E_p = 1880.4 keV. Resonant energies in Table 1 are believed accurate to ±3 keV except where larger errors are indicated. This uncertainty could have been reduced by taking a threshold each day, but this was not practical. The principal source of error in the remaining quantities in Table 1 is clear; the (p,α) yield indicates the presence of many more levels whose effects have been ignored. As discussed in Section A, the potential phase shifts, determined by the interaction radius, are based upon the observed cross section, primarily at the lower energies of the experiment. For the levels below 2.5 MeV, the partial widths should be accurate to 10 or 20%. For the levels above 2.5 MeV, errors in Γ_p and Γ_α could be somewhat larger. The estimate of the neutron partial widths is based upon the cross section of Blair and Leigh (1960); their uncertainty (±50%), compounded with the present ones would indicate that the estimate is no better than ± 70%.

Finally, the $^{16}O(p,p)^{16}O$ excitation function was measured for energies near the 2.66 MeV level (Figure 10). No fragmenting into any fine structure was observed. This level has a width of 19.9 keV and a spin and parity of $1/2^-$ (R. A. Laubenstein and M. J. W. Laubenstein, 1951). The difference between the ^{17}F and ^{19}F resonance structure is discussed in Chapter IV.

Figure 10. The $^{16}O(p,p)^{16}O$ Relative Yield Near the 2.66 MeV Level.

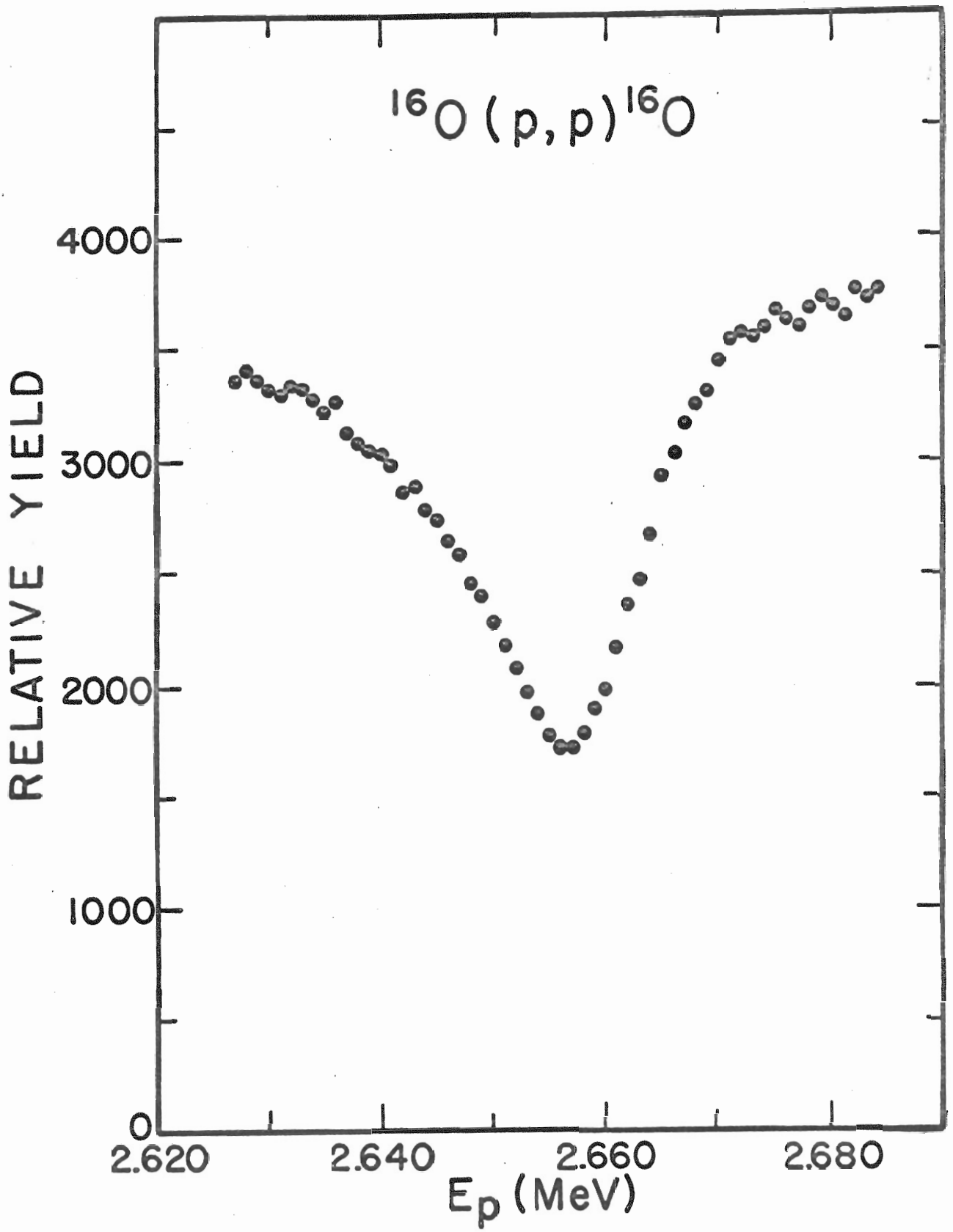
$^{16}O(p,p)^{16}O$
RELATIVE YIELD
4000
3000
2000
1000
0
2.620
2.640
2.660
2.680
E_p (MeV)

Chapter III

TWO PARTICLE ONE HOLE STATE CALCULATIONS

This model calculation, based on the doorway state concept, has been used by Beres and Divadeenam (1968) to study analog states in various medium-heavy nuclei. For the cases that they studied, it was necessary to calculate the damping widths for decay into 3p-2h states. It is shown in section B that in the present case all 3p-2h states are out of the experimental energy range. These states are not directly taken into account in the calculation; i.e., the diagonalization includes only 2p-1h configurations and damping widths are not calculated. The type of qualitative agreement obtained between model and experiment, discussed in the next chapter, is similar to that obtained by Afnan (1967) who likewise neglected the direct inclusion of these more complicated states in calculations on the A = 20 compound systems. His work deals with the $^{19}F(p,\gamma)^{20}Ne$ and $^{19}F(n,n)^{19}F$ cross sections.

A. Theory

The target nucleus or core with mass number A is pictured in its shell model ground state with closed subshells of Z protons and N neutrons.

Configuration mixing in the target ground state is neglected. The nucleus ^{18}O has two $1d_{5/2}$ neutrons outside the ^{16}O closed shells. Recent calculations show that, in fact, the ground state of ^{18}O consists of about 90% of this configuration (Cohan, Lawson, and MacFarlane, 1964). We treat this ground state configuration of ^{18}O as the core; this is done despite the fact that the $1d_{5/2}$ neutron shell is only partially filled. An alternative shell model description is to consider ^{16}O as the core. This requires calculating 3p-0h (rather than 2p-1h) states and obscures the analog doorway concept that we are trying to understand. We shall, at various times, refer to either a particle or a hole as a quasiparticle; thus the 2p-1h states discussed are alternatively called 3 quasiparticle states.

The Hamiltonian for the A + 1 system is

$$H = H_o + V, \tag{1}$$

where

$$H_o = \sum_{i=1}^{A+1} T_i + \sum_{i=1}^{A+1} U_i \ . \tag{2}$$

Here T_i is the usual kinetic energy of the i'th single particle and U_i is the average potential in which this particle moves. This single particle potential is taken to be a real Woods-Saxon well with real spin orbit coupling of the Thomas form plus the potential of a uniform sphere of charge Z. Thus H_o provides the single particle information. The residual interaction $V_{Res} = \frac{1}{2} \sum_{i=j} \mathcal{V}_{ij} - \sum_i U_i$ is replaced by an effective two body potential $V = \frac{1}{2} \sum_{i=j} v_{ij}$. For ease of calculation this is taken to have a delta function radial dependence with the Soper mixture. Thus the effective interaction between nucleons

i and j is

$$v_{ij} = -V_o \delta(\vec{r}_i - \vec{r}_j)(0.865 + 0.135\,\vec{\sigma}_i \cdot \vec{\sigma}_j) \quad , \tag{3}$$

where $\vec{\sigma}$ is twice the spin operator, $\vec{r}_i$ and $\vec{r}_j$ are the particle position vectors, and V_o is the strength. For two identical nucleons, $\vec{\sigma}_i \cdot \vec{\sigma}_j$ has the eigen value of -3; therefore,

$$v_{n_i n_j} = v_{p_i p_j} = -0.460\, V_o\, \delta\,(r_i - r_j) \quad , \tag{4}$$

where n and p refer to neutron and proton. The total two body interaction is

$$V = \frac{1}{2} \sum_{i=j} v_{p_i p_j} + \frac{1}{2} \sum_{i=j} v_{n_i n_j} + \sum_{ij} v_{n_i p_j}$$

$$= V_{pp} + V_{nn} + V_{np} \, . \tag{5}$$

The sums are over all the neutrons and protons in the system.

The calculation treats protons and neutrons as different particles. The presence of the Coulomb potential in H_o for protons produces radial wave functions different from those of neutrons. However, the effective two body Coulomb interaction is neglected in comparison with the effective two body nuclear interaction. The following discussion is quite general. Since the present experiment involves proton scattering, a proton is assumed incident on the target. All results are equally valid for an incident neutron if the roles of the odd proton and neutron are interchanged.

It is assumed, of course, that nuclear forces conserve parity. Accordingly, the calculation is done independently for states of a given spin and parity, J^{π}. Figure 11 indicates the three types of states involved.

Figure 11. The Three Types of States in the Calculation. In the symbol j_{pp}, the first p indicates it is a particle (rather than a hole) state while the second p indicates it is a proton (rather than a neutron) state. The notation of the other j's is similar (see text).

PROTON INCIDENCE ON TARGET

$|A\rangle =$ 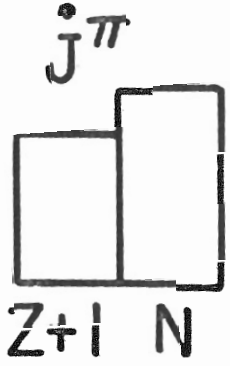

$= |\, J^\pi \,\rangle$

NEUTRON 2p 1h STATE

$|B\rangle =$ 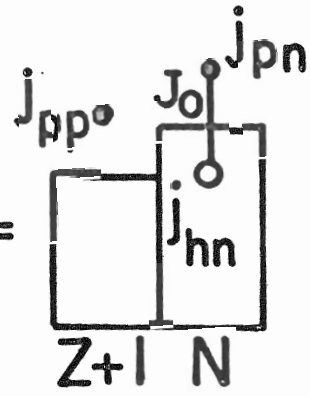

$= \left|\left[(j_{pn}, j_{hn})^{J_o}, j_{pp} \right]^{J^\pi} \right\rangle$

PROTRON 2p 1h STATE

$|C\rangle =$ 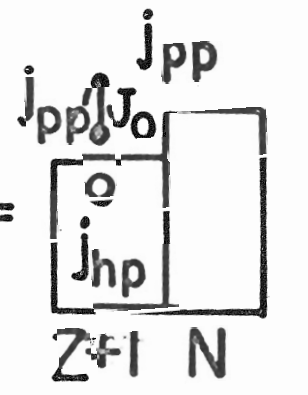

$= \left|\left[(j_{pp}, j_{pp'})^{J_o}, j_{hp} \right]^{J^\pi} \right\rangle$

The state $|A\rangle$ represents a proton in the continuum incident on the target. Unlike the other cases, it is not in any bound single particle state of the nucleus. However, since the state formed is to have spin and parity J^{π}, these quantum numbers correspond to state $|A\rangle$. Associated with each single particle state are the quantum numbers $n\ell j$ (e.g., $1d_{5/2}$); p or h for particle (empty) or hole (filled) subshell; and p or n for proton or neutron. No confusion arises by abbreviating this by the symbol j_{ab}, where j implies $n\ell j$, a is p or h for particle or hole, and b is p or n for proton or neutron. However, where obvious by context, the same symbol, e.g., j_{pn}, will also simply mean the value of j. This notation follows that of appendix B and of the programs written. Anyone seeking to work with these will appreciate this consistency. The state $|B\rangle$, then, represents a neutron 2p-1h state in which a single neutron is excited from a hole state in the core into a particle state above it. As indicated, these two quasiparticles are coupled to the intermediate spin J_o which in turn is coupled to j_{pp} to form the final J of the state. The parity of the state is, of course, the product of the parities of the single particle and hole states, i.e., $(-1)^{\ell_{pp}+\ell_{pn}+\ell_{hn}}$. Similarly, $|C\rangle$ represents a proton 2p-1h state in which a single proton has been excited by the incident proton. The spins of the two particle protons are first coupled to J_o. Finally, M, the projection of J, is physically undetermined and does not enter explicitly into any final expression; accordingly, it has been omitted.

Of course, the final results are independent of the intermediate

coupling scheme used and may be readily converted to any other. Note also that only bound single particle states are used in the construction of the 2p-1h states. The simple model involved here does not attempt to take into account interference effects between single particle and compound nucleus resonances.

Given the single particle and hole information, only certain 2p-1h states y_e of both kinds can form states of given spin and parity. If n such states can contribute, e runs from 1 to n. By physical assumption this set of n orthonormal states is complete; i.e., no other types of states are considered. These states are eigen states of H_o; thus,

$$H_o y_e = E_e^o y_e \quad . \tag{6}$$

The energy E_e^o of the 2p-1h state is given by

$$E_e^o = E_{pp} + E_{pb} - E_{hb} \quad , \tag{7}$$

where b is n or p for neutron or proton 2p-1h states respectively. Desired are the "doorway states" x_d which are eigen states of H; i.e.,

$$Hx_d = E_d x_d \quad . \tag{8}$$

These n states are linear combinations of the y_e's;

$$x_d = \sum_{e=1}^{n} u_{de} y_e \quad . \tag{9}$$

They are also orthonormal; thus,

$$(x_{d'}, Hx_d) = \delta_{dd'} E_d \quad , \tag{10}$$

where the inner product notation implies integration over spacial coordinates. The equations for obtaining the eigenvalues E_d and the coefficients u_{de} yielding the eigen states x_d are obtained by putting the expansion of x_d, equation (9), into equation (10) and replacing H by $H_o + V$, equation (1). These

equations are clearest in matrix form. The u_{de}'s form an n by n matrix U while the y_e's form an n dimensional vector Y. Thus,

$$U(E^o + \langle Y' | V | Y \rangle) \tilde{U} = E \ , \tag{11}$$

where $(U)_{de} = u_{de}$, $(E^o)_{ee'} = E^o_e \delta_{ee'}$, $(\langle Y' | V | Y \rangle)_{ee'} = (y_{e'}, V y_e)$, $(E)_{dd'} = E_d \delta_{dd'}$, and $\tilde{U}$ is the transpose of U. Thus the solution is obtained by diagonalizing the real symmetric matrix in parenthesis in equation (11) by the orthogonal transformation U. The matrix elements $(y_{e'}, V y_e)$ can be of the form (B', VB), (C', VC), or (B, VC) since y_e can be either a neutron or a proton 2p-1h state. These expressions are rather complicated and are presented in Appendix B.

As stated before, the diagonalization is done separately for states with spin and parity J^π. For completeness, the bound single particle proton state with this spin and parity may also be included in this diagonalization. If included, n, the number of basis states, is increased by one; and one of the y_e's is this bound single particle state. Its eigenvalue of H_o, equation (6), is just its single particle energy. The expressions for the matrix elements involving this state are identical to those used in calculating the widths of the doorway states. Calculation of these widths is described next.

The expression for the widths $\Gamma_d^{J^\pi}$ of the doorway states x_d is considered in detail by Beres and Divadeenam (1968). Basically, Fermi's golden rule is used to couple x_d to the continuum wave function $|A\rangle = |J^\pi\rangle$ at the energy of the doorway state via the effective interaction V. Thus,

$$\Gamma_d^{J^\pi} = \frac{4m}{\hbar^2 k} \left| (A, V x_d) \right|^2 , \tag{12}$$

where

$$(A, Vx_d) = \sum_{e=1}^{n} u_{de} (A, Vy_e) , \qquad (13)$$

by equation (9). Here m is the reduced mass and $\hbar k$ is the relative momentum of the incident proton and the target. The expressions for the matrix elements involved, (A, VB) and (A, VC), are in Appendix B. Note because A is a continuum wavefunction these matrix elements are complex numbers. If, as mentioned above, one of the y_e's is a bound single particle proton state, that state does not contribute to the width and may be omitted from the sum in equation (13).

B. Theoretical Results

The center of mass energies of the single particle and hole states based on ^{18}O as the core are given in Figure 12. Table 4 lists the well parameters used to generate these states and their wavefunctions. The diagonalization employs these states as contributors to the various possible 2p-1h configurations. Diagonalization of the complete set of 2p-1h states constructed from the above information was performed. It was found that only 2p-1h states including the $1d_{5/2}$ neutron hole state contributed in the energy range of the experiment. This is reasonable because the energies of the 2p-1h states involving deeper holes are out of our energy range; these states were excluded in further calculations.

The strength of the residual interaction (V_o in equation (3)) was

Figure 12. The Single Particle and Hole States of ^{18}O. The ground state of ^{18}O is the zero of energy. The negative of the hole energies are given. The $1d_{5/2}$ neutron hole energy (i.e., the binding energy of the last neutron in ^{18}O) was taken directly from the experimental evidence of Lauritsen and Selove (1962). The remaining energies were calculated from the well parameters of Beres and MacDonald (1967) for ^{16}O; the radii involved were increased proportionally to $A^{1/3}$. Scanning procedures in the computer program ABACUS (Auerbach, 1962) were used to determine these energies.

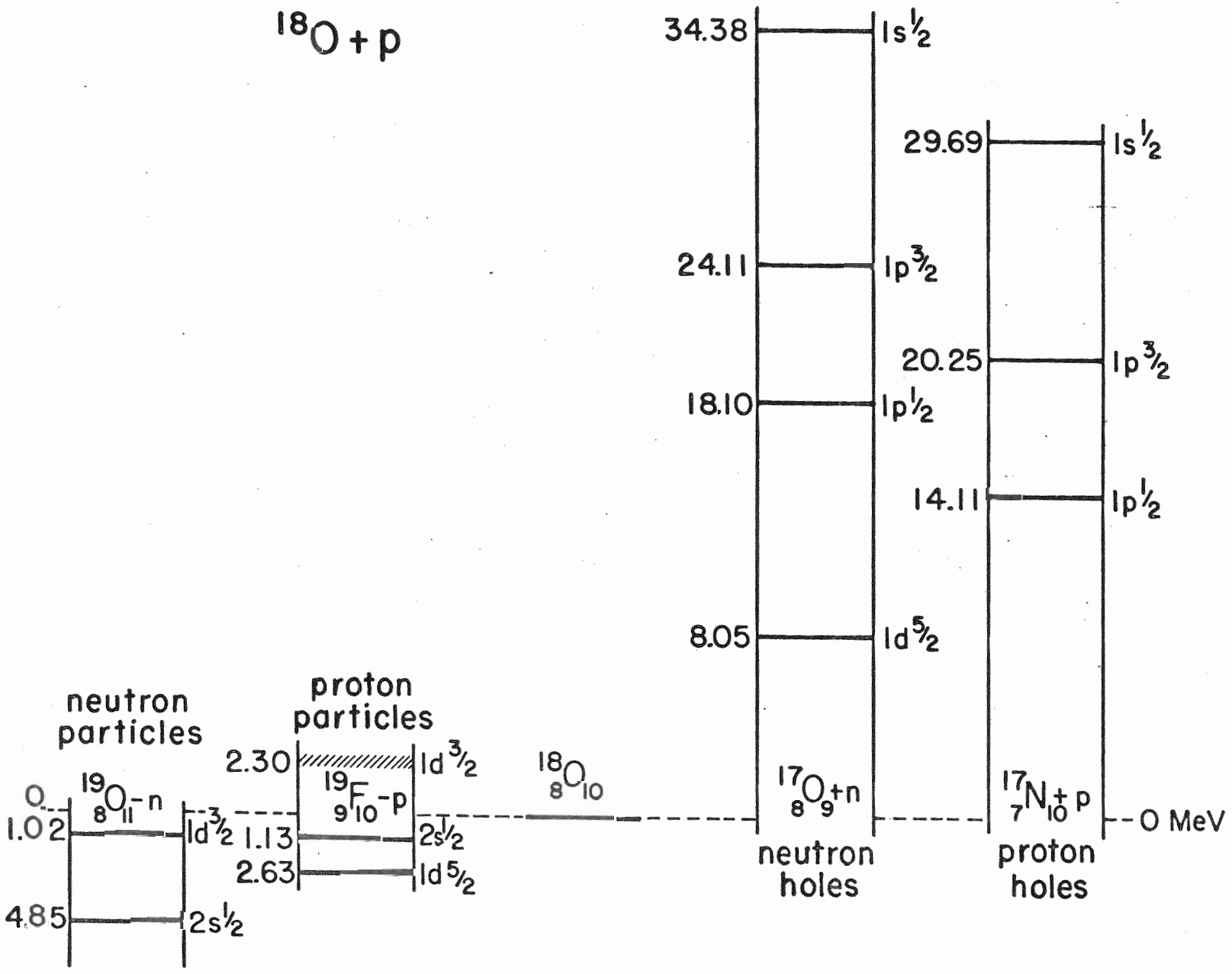
$^{18}O + p$
34.38
$1s_{1/2}$
29.69
$1s_{1/2}$
24.11
$1p_{3/2}$
20.25
$1p_{3/2}$
18.10
$1p_{1/2}$
14.11
$1p_{1/2}$
8.05
$1d_{5/2}$
neutron particles
proton particles
2.30
$1d_{3/2}$
$^{19}_{8}O_{11}$-n
$^{19}_{9}F_{10}$-p
$^{18}_{8}O_{10}$
$^{17}_{8}O_{9}$+n
$^{17}_{7}N_{10}$+p
0 MeV
0
1.02
$1d_{3/2}$
1.13
$2s_{1/2}$
2.63
$1d_{5/2}$
4.85
$2s_{1/2}$
neutron holes
proton holes

Table 4. Well Parameters for the Single Particle[/] and Hole[//] States

Neutron* State	E (MeV)	V_r (MeV)	Proton* State	E (MeV)	V_r (MeV)
$1d_{3/2}$	-1.02	50.0	$1d_{3/2}$	2.30	50.0
$2s_{1/2}$	-4.85	53.0	$2s_{1/2}$	-1.13	52.1
$1d^{-1}_{5/2}$	-8.05	57.0	$1d_{5/2}$	-2.63	50.0
$1p^{-1}_{1/2}$	-18.10	54.4	$1p^{-1}_{1/2}$	-14.11	53.9
$1p^{-1}_{3/2}$	-24.10	58.2	$1p^{-1}_{3/2}$	-20.25	57.9
$1s^{-1}_{1/2}$	-34.38	53.0	$1s^{-1}_{1/2}$	-29.70	52.1

[/] Proton (neutron) particle states are in $^{19}F(^{19}O)$.

[//] Proton (neutron) hole states are in $^{17}N(^{17}O)$.

* -1 indicates hole state

$$V(r)=\frac{-V_r}{1+\exp(\frac{r-R}{a})} - V_{so}\left(\frac{h}{2m_\pi}\right)^2 \frac{1}{r}\frac{d}{dr}\left[\frac{1}{1+\exp(\frac{r-R}{a})}\right] + V_c(r)$$

$$V_c(r) = \frac{Ze^2}{2R_c}\left(3 - \frac{r^2}{R_c^2}\right) \quad r \leq R_c$$

$$V_c(r) = \frac{Ze^2}{r} \quad r > R_c$$

$a = 0.5$ fm.

$r_o = 1.281$ fm. $\quad R = r_o A^{1/3}$

$V_{so} = 5.4$ MeV

$r_c = 1.345$ fm. $\quad R_c = r_c A^{1/3}$

initially put equal to its value in ^{16}O calculations (580 MeV fm.^{3}). Somewhat better overall agreement between the predicted levels and those observed in the experiment was obtained for slightly larger values; the value $V_o = 630$ MeV fm.^{3} was selected empirically.

Since (section A) unbound proton particle states are not used in the construction of 2p-1h levels, the predicted $1d_{3/2}$ single particle resonance at 2.30 MeV in the center of mass system (Table 4) is not included in the diagonalization. The calculated (ABACUS) width of this resonance is 100 keV. This state would not necessarily be seen experimentally because of interference with the compound nucleus resonances. The qualitative effects of this unbound state, within the framework of the present model, are discussed in the next chapter.

For completeness, single particle (i.e., 1p-0h) bound proton states of spins $1/2^+$ and $5/2^+$ were included in the diagonalizations; but their effects on the resulting energies, wavefunctions, and widths were found to be negligible. Thus, all calculated resonances are described simply in terms of 2p-1h doorway configurations.

The calculation of a width requires using a proton continuum wavefunction at the energy of the doorway state. Table 5 presents the center of mass energies and widths of all doorway states in the experimental range. The widths are presented for three specific well depths that were used to generate the continuum proton wavefunctions. The contributing 2p-1h states are listed in Table 6; the amplitudes of these doorways are given in Table 7.

Table 5. The Energies and Widths[/] of the ^{19}F Doorway States in the Range of the Experiment

E_d(c.m.) (MeV)	J^π	$\Gamma(V_r=50$ MeV) (keV)	$\Gamma(V_r=52.1$ MeV) (keV)	$\Gamma(V_r=60$ MeV) (keV)
2.23	$1/2^+$	224	153*	56.3
2.46	$3/2^+$	529*	13.2	0.58
1.58	$3/2^+$	67.8*	644	1.45
3.09	$5/2^+$	17.5*	13.4	6.50
2.30	$5/2^+$	0.98*	0.67	0.21
1.30	$5/2^+$	0.81*	0.47	0.09
1.00	$5/2^+$	0.26*	0.15	0.03

[/] Calculated for three different continuum proton well depths V_r.

* These widths are used in Figure 13 and are based on the well depths that generate the bound $1s_{1/2}$ and $1d_{5/2}$ proton states (cf. Table 4).

Table 6. The Contributing 2p-1h States in the Energy Range of the Experiment

	j_{pp}	j_{pn}	j_{hn}	J_o †	J ††	E^o (c.m.) (MeV)
1	$1d_{5/2}$	$2s_{1/2}$	$1d_{5/2}$	0	1/2	0.53
2	$1d_{5/2}$	$2s_{1/2}$	$1d_{5/2}$	1	1/2,3/2	0.53
3	$1d_{5/2}$	$2s_{1/2}$	$1d_{5/2}$	2	3/2,5/2	0.53
4	$1d_{5/2}$	$2s_{1/2}$	$1d_{5/2}$	3	5/2	0.53
5	$2s_{1/2}$	$2s_{1/2}$	$1d_{5/2}$	2	3/2,5/2	2.07
6	$2s_{1/2}$	$2s_{1/2}$	$1d_{5/2}$	3	5/2	2.07
7	$1d_{5/2}$	$1d_{3/2}$	$1d_{5/2}$	0	3/2	4.40
8	$1d_{5/2}$	$1d_{3/2}$	$1d_{5/2}$	1	1/2,3/2,5/2	4.40
9	$1d_{5/2}$	$1d_{3/2}$	$1d_{5/2}$	2	1/2,3/2,5/2	4.40
10	$1d_{5/2}$	$1d_{3/2}$	$1d_{5/2}$	3	3/2,5/2	4.40
11	$1d_{5/2}$	$1d_{3/2}$	$1d_{5/2}$	4	5/2	4.40
12	$2s_{1/2}$	$1d_{3/2}$	$1d_{5/2}$	2	1/2,3/2,5/2	5.90
13	$2s_{1/2}$	$1d_{3/2}$	$1d_{5/2}$	3	3/2,5/2	5.90

† The intermediate coupling scheme in which $\vec{J}_o = \vec{j}_{pp} + \vec{j}_{hn}$ is used. All parities are positive.

†† Values of $J > 5/2$ are excluded; all parities are positive.

Table 7

The Wavefunction Amplitudes* of the Doorway States

J^{π}	E_d (MeV) c.m.	1	2	3	4	5	6	7	8	9	10	11	12	13
$1/2^+$	2.23	-.071	.988	—	—	—	—	—	-.099	-.055	—	—	-.084	—
$3/2^+$	2.46	—	-.897	-.383	—	-.065	—	-.016	-.133	-.071	.115	—	-.116	.018
$3/2^+$	1.58	—	.408	-.870	—	-.247	—	-.046	-.096	-.000	-.015	—	-.055	.015
$5/2^+$	3.09	—	—	.081	.007	.352	-.124	—	.125	.285	.579	.624	-.083	-.160
$5/2^+$	2.30	—	—	-.644	-.305	-.497	-.415	—	.032	-.042	.046	.242	.059	.084
$5/2^+$	1.30	—	—	.716	-.271	-.329	-.546	—	-.046	-.008	.047	-.045	-.029	.007
$5/2^+$	1.00	—	—	-.013	-.856	.434	.142	—	-.076	-.166	-.095	-.019	.117	-.035

* The numbers 1 through 13 refer to the 2p-1h labeling scheme used in Table 6. A dash indicates that a particular 2p-1h state cannot contribute to a doorway of this spin.

For comparison to the doorway energies (center of mass), the available 3p-2h states below 7 MeV are listed in Table 8.

Table 8. Available 3p-2h States Below 7 MeV

J^{π}	E (c.m.) (MeV)	Number of 3p-2h States
$1/2^+$	3.66	1
$1/2^+$	5.16	1
$3/2^+$	3.66	2
$3/2^+$	5.16	1
$5/2^+$	3.66	3
$5/2^+$	5.16	1

Chapter IV

DISCUSSION

A. Comparison of Theory and Experiment

In this section, the experimental results are compared to those of the shell model calculations. The data is best illustrated in Figure 13; the experimental energies and proton elastic widths (Table 1) and theoretical energies and widths (Table 5) are compared. The energies of the doorway states have been converted to the laboratory system. Data taken by Yagi et al. (1962) below 1.4 MeV reveals that the elastic scattering in this region is dominated by a single s-wave level at 840 keV with a proton partial width of about 30 keV. This resonance is also included in Figure 13.

The $1/2^+$ doorway state at 2.35 MeV is in the vicinity of the three $1/2^+$ levels observed in the present experiment (Figure 13). From Table 1 it is seen that these three states also decay strongly through the alpha particle channels. The model state does not attempt to include components (4p-3h) that couple to the outgoing α-particle channels. Such complex configurations can mix with 3p-2h states (although these states are above 3.5 MeV as indicated in Table 8) which can themselves couple to the 2p-1h

Figure 13. Comparison of Experimental Resonances to Theoretical Doorway States. The calculated energies have been converted to laboratory values for comparison. Energies are given in MeV. The length of each line is proportional to the proton partial width of each resonance. Scale factors have been introduced for widths that are too large. The broken line indicates the $3/2^+$ or $5/2^+$ d-wave level.

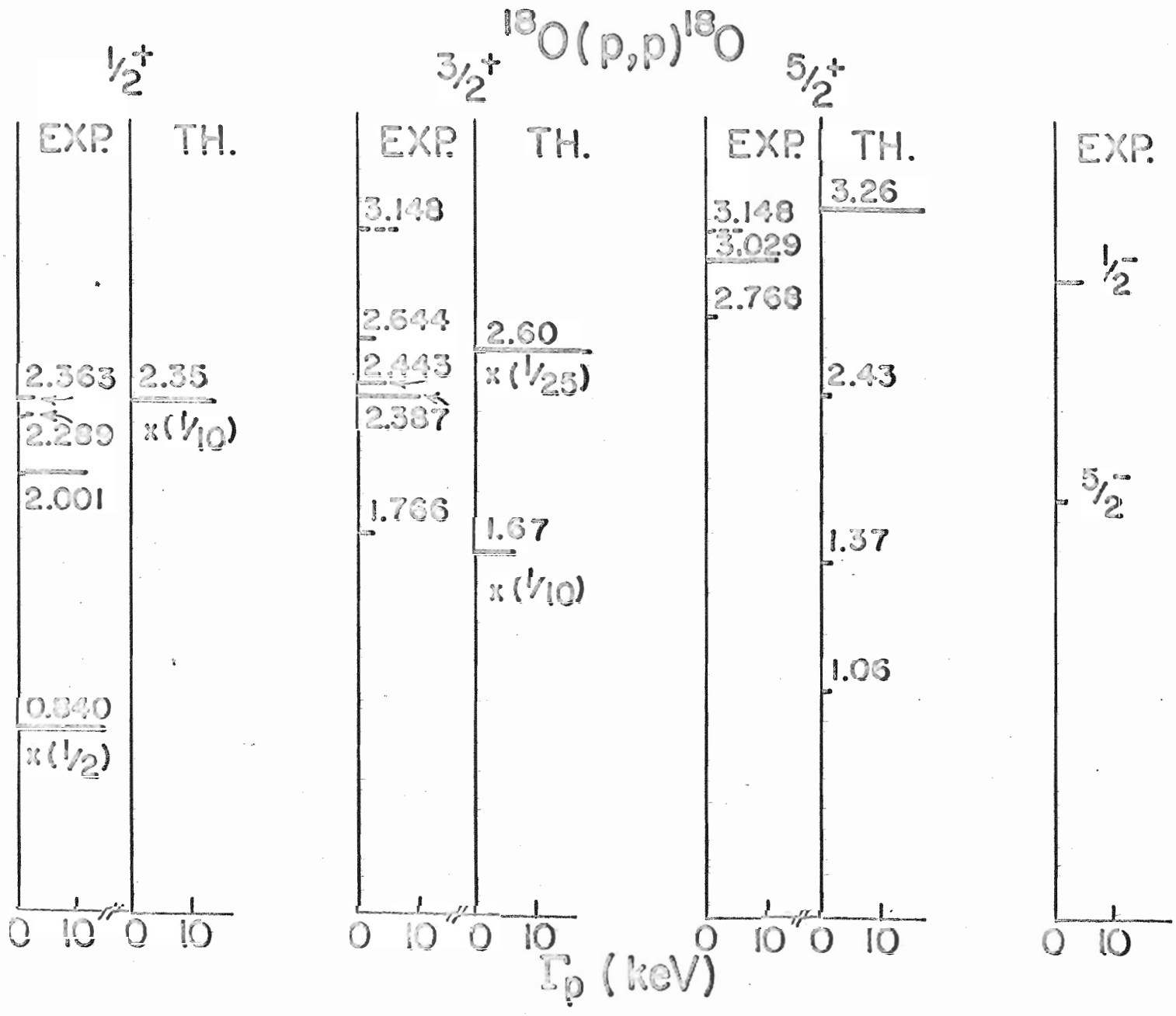
$^{18}O(p,p)^{18}O$
$1/2^+$
$3/2^+$
$5/2^+$
EXP.
TH.
EXP.
TH.
EXP.
TH.
EXP.
3.148
2.644
2.443
2.387
1.766
2.363
2.280
2.001
0.840
x(1/2)
2.35
x(1/10)
2.60
x(1/25)
1.67
x(1/10)
3.148
3.029
2.768
3.26
2.43
1.37
1.06
1/2
5/2
0 10 0 10
0 10 0 10
0 10 0 10
0 10
Γ_p (keV)

doorway. If these more complicated excitations were included, the doorway state would be fragmented. It is not unreasonable then to associate the three observed resonances with the theoretical doorway state. If the 4p-3h states were to coalesce into an α-particle cluster in the nucleus (the binding energy for an α-particle is 28 MeV), then such states would be within the energy range of the experiment. Although no detailed study is attempted here, this provides a possible explanation of the α-particle yield, and discrepancies between theoretical and experimental widths.

The sum of the three observed proton partial widths is 17 keV, while calculated values range from 224 to 56.3 keV. From Table 5, it is seen that the best agreement comes from a 60 MeV well depth for the continuum proton wavefunction. Deeper wells would lead to better agreement. However, optical model calculations in the literature indicate that well depths deeper than about 60 MeV are unreasonable.

In a similar way it is reasonable to associate the three $3/2^+$ levels found experimentally above 2 MeV (and possibly the d-wave at 3.148 MeV) with the $3/2^+$ doorway state at 2.60 MeV. In addition, the $3/2^+$ model state at 1.67 MeV lines up very well with the remaining $3/2^+$ level observed experimentally. The calculated doorway widths for $3/2^+$ (Figure 13) are larger by factors of about 30 than those of the associated experimental levels. Different assumed values of the well depth for the continuum proton wavefunction drastically change the values of the calculated widths (Table 5); in fact, a well depth of 60 MeV reduces the width of the 2.60 MeV doorway to a

negligible value while that of the 1.67 MeV doorway is reduced to 1.5 keV. This highly eratic behavior is best interpreted in terms of the unbound, 100 keV wide, $1d_{3/2}$, calculated, proton single particle resonance mentioned in Chapter III. The continuum wavefunction varies rapidly with energy near such a resonance, and the resonant energy of the single proton level decreases as the well depth is increased. For the present case, it was found that increasing the well depth 2 MeV decreased the resonant energy about 1 MeV. From Table 4, a real well depth of 50.0 MeV yields a resonant energy of 2.42 MeV (laboratory system). Thus, for a real well depth V_r = 50.0 MeV, the resonance is near the 2.60 MeV doorway; for V_r = 52.1 MeV, the resonance is near the 1.67 MeV doorway; for V_r = 60.0 MeV, the $1d_{3/2}$ proton state is bound at 3 MeV. Referring to Table 5, two facts are noted: One, the width of each doorway state becomes unrealistically large if the calculated single proton resonance is near. Two, the ratio of the sizes of the two theoretical widths (529/67.8 = 7.8) agrees well with the corresponding ratio (18.6/2.1 = 8.9) of the widths of the associated experimental levels for V_r = 50 MeV.

Continuing in the above manner, the strong $5/2^+$ experimental level at 3.029 MeV is associated with the doorway state at 3.26 MeV (Figure 13). Interpretation of the 3.148 MeV level is most natural as an additional fragment of this doorway state; however, this would require a spin assignment of 5/2 to this d-wave level which is uncertain. It is not clear whether the weak $5/2^+$ level at 2.768 MeV should be interpreted as an additional fragment of this doorway state or as a fragment of the 2.43 MeV doorway. For

any of the various possible combinations, agreement between calculated and observed widths is quite good (Figure 13). In particular, from Table 5 the theoretical width of the 3.26 MeV doorway is 17.5 keV (V_r = 50 MeV) while that of the associated strong experimental level is 13 keV; The calculated width of the 2.43 MeV doorway is 1 keV while that of the 2.768 MeV observed resonance is 0.7 keV.

The widths of the theoretical $5/2^+$ doorways at 1.37 and 1.06 MeV are 0.8 and 0.3 keV respectively. Any possible remaining fragments of the 2.43 MeV doorway state, or fragments of the $5/2^+$ doorway states at lower energies would produce levels with small proton partial widths. The large positive Q-value for α-particle decay (3.998 MeV) causes large (charged particle) penetration factors. (The penetration factor for $\ell = 5$ α-particle decay exceeds that for $\ell = 0$ proton decay throughout the energy range of the experiment.) Thus, from penetrability arguments, the presence of levels with $\Gamma_p << \Gamma_\alpha$ is highly favored, particularly at lower energies. Such levels produce very small anomalies in both the elastic and the (p, α) yields. Under these circumstances, any effects of these narrow doorway states may be very difficult to determine experimentally. As indicated in Figure 13, no additional d-wave levels were identified in the present experiment.

The present calculation does not explain the $1/2^+$ resonance at 840 keV or the negative parity resonances. A possible interpretation of the former is that it is formed by coupling the 2^+ excited state in ^{18}O at 2 MeV with the $1d_{3/2}$ and $1d_{5/2}$ single proton states. In the latter case a possible

mechanism is to couple the (3^-) level in ^{18}O at 4.5 MeV with these single proton states. An alternate explanation is to include alpha particle clusters, i.e., 4p-3h states with respect to ^{18}O. A general calculation taking these additional effects into account would be quite complicated and has not been attempted here. However, the simple 2p-1h model does interpret most levels with strong proton widths in our experimental energy range.

B. Possible Analogue Levels

To determine the properties of states in ^{19}O, the reactions $^{17}O(t,p)^{19}O$ and $^{18}O(d,p)^{19}O$ have been investigated quite recently by Wiza and Middleton (1966); similarly, the (t,p) reaction has been investigated by Moreh (1965). In particular, levels at excitation energies of 1.47 and 3.16 MeV (c.m.) have been observed; these have spins and parities of $1/2^+$ and $5/2^+$ and relative reduced widths of 1.0 and 0.035 respectively (Wiza and Middleton, 1966). The 840 keV s-wave resonance in ^{19}F has been identified as the "analogue" of the $1/2^+$ state in ^{19}O by Prosser et al. (1967); however, if this resonance were a pure $T = 3/2$ analogue state, α-particle decay (requiring $T = 1/2$) would be absent. In fact, Carlson et al. have observed strong α-particle decay due to this resonance. (Their fit to the elastic data requires $\Gamma_\alpha = 20$ keV.) Thus this interpretation of the 840 keV s-wave also requires large admixtures of $T = 1/2$ components in its wavefunction. Based upon the position of the $1/2^+$ state at 840 keV, the analogue of the $5/2^+$ state would be expected near $E_p = 2.6$ MeV. The small reduced width

of the ^{19}O $5/2^+$ state implies that its analogue would have a small proton partial width. The pure analogue state would only decay through the elastic and inelastic proton channels (neutron decay also requires $T = 1/2$). However, if large admixtures of $T = 1/2$ are also present in the analogue wavefunction, the $5/2^+$ level observed in all decay channels at 2.768 MeV - with its small proton partial width - could be, at least in part, the so called analogue of the $5/2^+$ state in ^{19}O.

In Table 6 it is seen that only states 1 and 7 are of the usual 2p-1h type for the description of $1/2^+$ and $3/2^+$ analog resonances respectively (i.e., $j_{pp} = j_{hn}$ and $J_o = 0$). However, these states do not contribute significantly to any of the doorways (Table 7). For $5/2^+$ it is helpful to rewrite the doorway wavefunctions in an intermediate coupling scheme which is more transparent for the present case; viz., $J_o' = j_{pp} + j_{pn}$ (Tables 9 and 10). One notes that the 2p-1h doorway numbered 3 in Table 9 consists of both the proton and neutron particles in $2s_{1/2}$ states coupled to 0; the spin of this component can only be 5/2 since it is determined by the neutron hole. Equivalently, this component can be pictured in terms of three particles with ^{16}O as the inert core; in this description, the spin of the component is determined by the single neutron in the $1d_{5/2}$ state while the proton and other neutron are in $2s_{1/2}$ states and are coupled to 0. This identical configuration can be formed by the three neutrons in ^{19}O by simply changing the $2s_{1/2}$ proton into a neutron; Moreh (1965) determined that this configuration is the most probable for the $5/2^+$ state at 3.16 MeV in ^{19}O. Referring to Table 10; it

Table 9.[f] The Contributing 2p-1h States in the Intermediate Coupling Scheme $\vec{J}_o = \vec{j}_{pp} + \vec{j}_{pn}$

	j_{pp}	j_{pn}	j_{hn}	J_o'	E^o(MeV) (c.m.)
1	$1d_{5/2}$	$2s_{1/2}$	$1d_{5/2}$	2	0.53
2	$1d_{5/2}$	$2s_{1/2}$	$1d_{5/2}$	3	0.53
3	$2s_{1/2}$	$2s_{1/2}$	$1d_{5/2}$	0	2.07
4	$2s_{1/2}$	$2s_{1/2}$	$1d_{5/2}$	1	2.07
5	$1d_{5/2}$	$1d_{3/2}$	$1d_{5/2}$	1	4.40
6	$1d_{5/2}$	$1d_{3/2}$	$1d_{5/2}$	2	4.40
7	$1d_{5/2}$	$1d_{3/2}$	$1d_{5/2}$	3	4.40
8	$1d_{5/2}$	$1d_{3/2}$	$1d_{5/2}$	4	4.40
9	$2s_{1/2}$	$1d_{3/2}$	$1d_{5/2}$	1	5.90
10	$2s_{1/2}$	$1d_{3/2}$	$1d_{5/2}$	2	5.90

[f] Except for J_o', the same symbols are used in Table 6

Table 10. Doorway Wavefunction Amplitudes[/] for $J = 5/2^+$

E_d(MeV) (c.m.)	1	2	3	4	5	6	7	8	9	10
3.09	-.047	-.066	-.133	-.349	-.899	.088	.067	-.034	-.179	.024
2.30	.586	.405	.637	.112	-.175	.166	-.057	-.047	-.035	.096
1.30	-.123	-.756	.630	-.101	.013	-.017	.077	.006	-.011	-.028
1.00	.748	-.417	-.389	-.240	.154	.133	.019	-.033	.039	.116

[/] The numbers 1 through 10 refer to the 2p-1h labeling scheme in Table 9.

is seen that while other components contribute, the 2p-1h state numbered 3 is the largest ingredient of the 2.30 MeV (c.m.) doorway. This component also contributes strongly to the 1.30 MeV (c.m.) doorway; however, the largest ingredient of this state is the one numbered 2 in Table 9. The observed resonance at 2.768 MeV has approximately the same energy as the expected $5/2^+$ analogue. One may conjecture that it is the analogue state - although impure - and associate it with the calculated doorway at the lab. energy of 2.43 MeV (cf. Figure 13).

C. Comparison with Other Light Nuclei

It is interesting to compare the details of the experimental spectra for ^{19}F with those seen in the same experimental range in ^{17}F and ^{23}Na. As mentioned at the end of Chapter II, the ^{17}F data indicates that there are no positive parity resonances (only a single $1/2^-$ level has been observed), while in ^{23}Na (Keyworth, 1968) about 75 resonances of both parities are observed. The indication is that the ^{19}F resonance structure is intermediate in complexity between those of ^{17}F and ^{23}Na. The latter has seven nucleons outside of the ^{16}O core whereas the former has just one proton outside of this core. The importance of the availability of various particle hole configurations for determining the amount of fine structure is clearly demonstrated in these two disparate cases.

APPENDIXES

Appendix A

R-MATRIX FORMULAE AND PROGRAM

The program MULTI computes R-matrix cross sections for cases in which several channels may be open and several levels may be interfering with one another. Under other circumstances, the programmed formulae reduce to simpler expressions, most notably the Breit-Wigner single level formulae. This reduction was demonstrated by Blatt and Biedenharn (1952). The more general formulae are written here in the notation of Lane and Thomas (1958). Our major concern is practical computation based on these formulae. With this in mind, some of the notation is discussed briefly.

The compound nucleus decays via various pairs of nuclei. To be specific, the observed "particle" is numbered 1; the residual "nucleus" is numbered 2. Information for each particle is input to the program on this basis, except where it is clear that only relative quantum numbers are of consequence. For example, a channel c is specified by the quantities J^π, a, s, ℓ. The spin and parity of the two particles is J^π. The properties of these two separated particles (quantum numbers, masses, charges, etc.) are specified by a. The spins I_1 and I_2 of the two particles sum to s. Their relative orbital momentum is ℓ.

Only channels with positive energies are considered. Capture of particles leading to γ-decay is neglected. Hard sphere phase shifts, determined by the interaction radii, are used. Even under these assumptions, over 700 interrelated parameters can be varied. In order to allow investigation of the numerous possibilities, every effort was made to reduce computation time. Toward this end, the "slowly varying" quantities ϕ, S, and P are interpolated (quadratically) for charged particles. These quantities are calculated from Coulomb wave functions generated in the subroutine EXTFN which was written by M. L. Gursky at Los Alamos Scientific Lab.

The R-matrix is obtained by the usual relation,

$$R_{cc'} = \sum_{\lambda} \frac{\gamma_{\lambda c} \gamma_{\lambda c'}}{E_{\lambda} - E} \quad .$$

The sum is over the levels of the compound system labeled by λ. U, the scattering matrix, is given by

$$U = \Omega L P^{1/2} (1 - RL_o)^{-1} (1 - RL_o^{*}) P^{1/2} \Omega \quad .$$

Here "*" denotes complex conjugate. As indicated, the complex matrix $1 - RL_o$ is inverted. Next, the T-matrix is obtained.

$$T_{cc'} \equiv T^{J^{\pi}}_{\alpha' s' \ell'; \alpha s \ell} = e^{2i\omega_{\alpha'\ell'}} \delta_{\alpha' s' \ell'; \alpha s \ell} - U^{J^{\pi}}_{\alpha' s' \ell'; \alpha s \ell} \quad .$$

The formula for the differential cross section describing pair α incident with channel spin s and pair α' outgoing with channel spin s' in terms of the T-matrix is

$$\frac{d\sigma_{\alpha s;\alpha' s'}}{d\Omega_{\alpha'}} = \frac{\pi}{K_\alpha^2}\left|C(\theta_\alpha)\right|^2 \delta_{\alpha' s';\alpha s}$$

$$+ \frac{\sqrt{\pi}}{K_\alpha^2(2s+1)} \sum_{J^\pi \ell} \left[(2J+1) P_\ell(\cos\theta_\alpha)\, \mathrm{Re}\left(i T^{J^\pi *}_{\alpha' s' \ell';\alpha s \ell}\, C_\alpha(\theta_\alpha)\right)\right] \delta_{\alpha' s';\alpha s}$$

$$+ \frac{1}{K_\alpha^2(2s+1)} \sum_L B_L(\alpha' s';\alpha s)\, P_L(\cos\theta_{\alpha'}).$$

Here

$$C_\alpha(\theta_\alpha) = \frac{n_\alpha}{\sqrt{4\pi}}\, e^{-2i\eta_\alpha \log(\sin\theta_\alpha/2)}$$

and

$$B_L(\alpha' s';\alpha s) = \frac{(-1)^{s'-s}}{4} \sum_{\substack{J_1^\pi J_2^\pi \\ \ell_1 \ell_1' \ell_2 \ell_2'}} \bar{Z}(\ell_1, J_1, \ell_2, J_2; s L)$$

$$\bar{Z}(\ell_1', J_1, \ell_2', J_2; s' L)\, T^{J_1^\pi *}_{\alpha' s' \ell_1';\alpha s \ell_1}\, T^{J_2^\pi}_{\alpha' s' \ell_2';\alpha s \ell_2}.$$

Numerous conditions given by Biedenharn, Blatt, and Rose (1952) are used to reduce the number of terms in the last sum.

Also programmed are the formulae for cross sections summed over the channel spins s' of the outgoing particles. Thus the cross section

$$\frac{d\sigma_{\alpha s;\alpha'}}{d\Omega_{\alpha'}} = \frac{(2s+1)}{(2I_1+1)(2I_2+1)} \sum_{s'} \frac{d\sigma_{\alpha s;\alpha' s'}}{d\Omega_{\alpha'}}$$

can be computed directly; similarly, the total cross section (integrated over angle)

$$\sigma_{\alpha s;\alpha'} = \frac{4\pi}{(2I_1+1)(2I_2+1)k_\alpha^2} \sum_{s'} B_0(\alpha' s';\alpha s)$$

can be computed. While sums over incident channel spins cannot be directly computed, the necessary cross sections can be output separately.

The program MULTI has been used to analyze data for a proton incident on targets with zero spin. It must be emphasized that this assumption is nowhere made in the program. This generality can lead to two possible pitfalls in the input procedure. One, care must be taken to include all J^{π}'s for which (non-Rutherford) potential scattering is significant. Two, sums over outgoing channel spins are meaningful only if the program has previously computed the relevant cross sections.

All programming was done in FORTRAN IV "H-level" on the TUCC IBM 360-75 computer. No difficulty was encountered during development of the program despite numerous changes in the "system" on which it was developed.

The calculation, controlled by the subroutine MULTI, employes several additional subprogrammes (INV, TMATRX, ZB, FILL, BSUBL, SIGMA). Data control is handled by the MAIN program. Input statements are sequentially listed in MAIN and MULTI, except for energy resolution considerations (SMEAR).

Current (the program can easily be modified) DIMENSION statements allow 35 channels, 20 levels, 7 different J^{π} values, values of $\ell \leq 4$, 600 data pts., and 400 calculation pts. (both data and calculated points can be in variable energy steps.) These restrictions require 180 K bytes of core storage; extension of the range of the above values can be obtained if larger core storage is readily available.

Appendix B

MATRIX ELEMENTS

In this appendix, the expressions are given for the matrix elements (B', VB), (C', VC), (C', VB), (A, VB) and (A, VC) mentioned in Chapter III, Section A. States $|A\rangle$, $|B\rangle$ and $|C\rangle$ are given in Figure 11. In addition,

$$|B'\rangle = |[(j_{pn'}, j_{hn'})^{J_0'}, j_{pp'}]^{J^\pi}\rangle, \tag{B.1}$$

and

$$|C'\rangle = |[(j_{pp''}, j_{pp'''})^{J_0'}, j_{hp'}]^{J^\pi}\rangle. \tag{B.2}$$

The interaction V is given by equation (5).

The following notation is used. The Kronecker delta $\delta_{pp,pp'} = 0$ unless $n_{pp} = n_{pp'}$, $\ell_{pp} = \ell_{pp'}$, $j_{pp} = j_{pp'}$. Other Kronecker notation is similar.

The symbol $(j_1\, m_1\, j_2\, m_2 | j_3\, m_3)$ is a vector coupling coefficient; $\begin{Bmatrix} j_1 & j_2 & j_3 \\ j_4 & j_5 & j_6 \end{Bmatrix}$ is a 6 - j symbol; $\begin{Bmatrix} j_1 & j_2 & j_3 \\ j_4 & j_5 & j_6 \\ j_7 & j_8 & j_9 \end{Bmatrix}$ is a 9 - j symbol (see Edmonds, 1957).

The symbol $F^{pn,\, pn',\, hn,\, hn'} = \frac{1}{4\pi} \int_0^\infty r^{-2}\, U_{pn}\, U_{pn'}\, U_{hn}\, U_{hn'}\, dr$ where $U = rR$; R is the solution of the radial Schrodinger equation. Notation for other F's is similar.

An alternate way to write the delta function interaction in equation (3) is

$$v_{ij} = - V_o\, \delta(r_i - r_j)\, (\pi_t + P\, \pi_s)$$

where

$$\pi_t = \frac{1}{4}\, (3 + \vec{\sigma}_i \cdot \vec{\sigma}_j)\,,$$

and

$$\pi_s = \frac{1}{4}\, (1 - \vec{\sigma}_i \cdot \vec{\sigma}_j)$$

are the spin-triplet and spin-singlet projection operators respectively, and P is the ratio of singlet to triplet strength. In the following expressions, one uses $P = 1$ for V_{nn} and V_{pp}, and $P = 0.460$ for V_{np}.

1) The matrix element (B', VB):

$$\langle B' | V_{pp} | B \rangle = 0. \tag{B.3}$$

$$\langle B' | V_{hn} | B \rangle = 0.46 \frac{V_0 F^{pn, pn', hn, hn'}}{2 (2 J_0 + 1)} \delta_{pp, pp'} \delta_{J_0, J_0'}$$

$$\hat{j}_{pn'} \hat{j}_{hn} \hat{j}_{pn} \hat{j}_{hn'} (-1)^{j_{pn} + j_{pn'} + \ell_{pn} + \ell_{pn'}} \left[1 - \right.$$

$$\left. \frac{(1-P)}{2} \left(1 + (-1)^{\ell_{hn'} + \ell_{pn} + \ell_{pn'} + \ell_{hn}} \right) \right] \left[(-1)^{j_{pn} + j_{pn'}} \right.$$

$$\left(j_{hn'} \tfrac{1}{2} \; j_{pn'} \tfrac{1}{2} \mid J_0 \, 1 \right) \left(j_{hn} \tfrac{1}{2} \; j_{pn} \tfrac{1}{2} \mid J_0 \, 1 \right) + (-1)^{\ell_{hn'} + \ell_{pn} + J_0}$$

$$\left. \left(j_{hn'} \tfrac{1}{2} \; j_{pn'} -\tfrac{1}{2} \mid J_0 \, 0 \right) \left(j_{hn} \tfrac{1}{2} \; j_{pn} -\tfrac{1}{2} \mid J_0 \, 0 \right) \right]. \tag{B.4}$$

$$\langle B' | V_{np} | B \rangle = \frac{V_0 F^{pp, pp', pn, pn'}}{2} (-1)^{J_0 + J_0' + j_{pp'} + j_{pp}}$$

$$\delta_{hn, hn'} \hat{j}_{pn'} \hat{j}_{pp'} \hat{j}_{pn} \hat{j}_{pp} \hat{J}_0 \hat{J}_0' \sum_K \begin{Bmatrix} J & j_{hn} & K \\ j_{pn'} & j_{pp'} & J_0' \end{Bmatrix}$$

$$\begin{Bmatrix} J & j_{hn} & K \\ j_{pn} & j_{pp} & J_0 \end{Bmatrix} \left(\left(j_{pn'} -\tfrac{1}{2} \; j_{pp'} -\tfrac{1}{2} \mid K \, -1 \right) \left(j_{pn} -\tfrac{1}{2} \; j_{pp} -\tfrac{1}{2} \mid K \, -1 \right) \right.$$

$$+\left[(-1)^{j_{pn}+j_{pn'}+\ell_{pn}+\ell_{pn'}+1}\left(j_{pn'}\ \tfrac{1}{2}\ j_{pp'}\ -\tfrac{1}{2}\,|\,K\,0\right)\right.$$

$$\left.\left(j_{pn}\ \tfrac{1}{2}\ j_{pp}\ -\tfrac{1}{2}\,|\,K\,0\right)\right]\left[1-(1-P)\left(\frac{1+(-1)^{\ell_{pn'}+\ell_{pp'}+K}}{2}\right)\right]\Bigg)$$

$$+\frac{V_0\,F^{pp,\,pp',\,hn,\,hn'}}{2}\,(-1)^{j_{pp'}+j_{pp}+j_{hn}+j_{hn'}}\,\delta_{pn,\,pn'}$$

$$\hat{j}_{hn}\ \hat{j}_{pp'}\ \hat{j}_{hn'}\ \hat{j}_{pp}\ \hat{J}_0\ \hat{J}_0'\ \sum_K \begin{Bmatrix} j_{pn} & j_{hn'} & J_0' \\ j_{hn} & K & j_{pp'} \\ J_0 & j_{pp} & J \end{Bmatrix}$$

$$\Bigg(\left(j_{hn}\ -\tfrac{1}{2}\ j_{pp'}\ -\tfrac{1}{2}\,|\,K\,-1\right)\left(j_{hn'}\ -\tfrac{1}{2}\ j_{pp}\ -\tfrac{1}{2}\,|\,K\,-1\right)$$

$$+\left[(-1)^{j_{hn'}+j_{hn}+\ell_{hn'}+\ell_{hn}+1}\left(j_{hn}\ \tfrac{1}{2}\ j_{pp'}\ -\tfrac{1}{2}\,|\,K\,0\right)\right.$$

$$\left.\left(j_{hn'}\ \tfrac{1}{2}\ j_{pp}\ -\tfrac{1}{2}\,|\,K\,0\right)\right]\left[1-(1-P)\left(\frac{1+(-1)^{\ell_{hn}+\ell_{pp'}+K}}{2}\right)\right]\Bigg) \quad \text{(B.5)}$$

2) The matrix element (C', VC):

$$\langle c' | V_{pn} | c \rangle = \langle c' | V_{nn} | c \rangle = 0. \tag{B.6}$$

$$\langle c' | V_{pp} | c \rangle = \left[(1 + \delta_{pp'', pp'''})(1 + \delta_{pp, pp'}) \right]^{-1/2}$$

$$\delta_{hp, hp'} \delta_{J_0, J_0'} \left[\langle (j_{pp''}, j_{pp'''})^{J_0} | V_{pp} | (j_{pp}, j_{pp'})^{J_0} \rangle \right.$$

$$\left. -(-1)^{j_{pp} + j_{pp'} + J_0} \langle (j_{pp''}, j_{pp'''})^{J_0} | V_{pp} | (j_{pp'}, j_{pp})^{J_0} \rangle \right]$$

$$+ (2J+1) \hat{J}_0 \hat{J}_0' \sum_K (-1)^K (2K+1) \left[D - (-1)^{j_{pp} + j_{pp'} + J_0} \right.$$

$$D \text{ (with } j_{pp} \text{ and } j_{pp'} \text{ interchanged)} - (-1)^{j_{pp''} + j_{pp'''} + J_0'}$$

$$\left. D \text{ (with } j_{pp''} \text{ and } j_{pp'''} \text{ interchanged)} + (-1)^{j_{pp} + j_{pp'} + j_{pp''} + j_{pp'''} + J_0 + J_0'} \right.$$

$$\left. D \text{ (with } j_{pp} \text{ and } j_{pp'} \text{ interchanged and } j_{pp''} \text{ and } j_{pp'''} \text{ interchanged)} \right].$$

(B.7)

Here

$$D = -\frac{\delta_{pp,pp'''}(-1)^{j_{pp''}+J+J_0}}{\sqrt{(1+\delta_{pp'',pp})(1+\delta_{pp,pp'})}} \begin{Bmatrix} j_{pp''} & j_{pp} & J_0' \\ K & j_{pp'} & j_{hp} \\ j_{hp} & J_0 & J \end{Bmatrix}$$

$$\left[\langle (j_{pp''}, j_{hp})^K | V_{pp} | (j_{pp'}, j_{hp'})^K \rangle - (-1)^{j_{pp'}+j_{hp'}+K} \right.$$

$$\left. \langle (j_{pp''}, j_{hp})^K | V_{pp} | (j_{hp'}, j_{pp'})^K \rangle \right], \qquad \text{(B.8)}$$

and

$$\langle (j_{1p}, j_{2p})^K | V_{pp} | (j_{1p'}, j_{2p'})^K \rangle = -0.46 V_0 \frac{\delta_{1p,2p,1p',2p'}}{2(2K+1)}$$

$$\hat{j}_{1p}\,\hat{j}_{2p}\,\hat{j}_{1p'}\,\hat{j}_{2p'} \Big((j_{1p}\,-1/2\;\; j_{2p}\,-1/2 \,|\, K\,-1)(j_{1p'}\,-1/2\; j_{2p'}\,-1/2 \,|\, K\,-1)$$

$$+ (-1)^{j_{1p'}+j_{1p}+l_{1p'}+l_{1p}+1} (j_{1p}\,1/2\; j_{2p}\,-1/2 \,|\, K\,0)$$

$$(j_{1p'}\,1/2\;\; j_{2p'}\,-1/2 \,|\, K\,0)\left[1-(1-P)\left(\frac{1+(-1)^{l_{1p}+l_{2p}+K}}{2}\right)\right] \Big). \qquad \text{(B.9)}$$

3) The matrix element (C', VB):

$$\langle C' | V_{nn} | B \rangle = \langle C' | V_{pp} | B \rangle = 0. \qquad \text{(B.10)}$$

$$\langle C' | V_{np} | B \rangle = \hat{J}_0 \hat{J}_0' (-1)^{j_{hn} + j_{hp'} + J_0} \left[\delta_{pp',p'p''} \frac{1}{\sqrt{1+\delta_{pp'';pp}}} \right.$$

$$\begin{Bmatrix} J & J_0 & j_{pp} \\ j_{pp'''} & J_0' & j_{hp'} \end{Bmatrix} \sum_K (-1)^K (2K+1) \begin{Bmatrix} j_{pp'''} & j_{hp'} & J_0 \\ j_{pn} & j_{hn} & K \end{Bmatrix}$$

$$\langle (j_{hn}, j_{pp'''})^K | v_{np} | (j_{pn}, j_{hp'})^K \rangle - (-1)^{j_{pp''} + j_{pp} + J_0'} \delta_{pp';pp'''}$$

$$\frac{1}{\sqrt{1+\delta_{pp'';pp}}} \begin{Bmatrix} J & J_0 & j_{pp} \\ j_{pp''} & J_0' & j_{hp'} \end{Bmatrix} \sum_K (-1)^K (2K+1) \begin{Bmatrix} j_{pp''} & j_{hp'} & J_0 \\ j_{pn} & j_{hn} & K \end{Bmatrix}$$

$$\left. \langle (j_{hn}, j_{pp''})^K | v_{np} | (j_{pn}, j_{hp'})^K \rangle \right], \qquad \text{(B.11)}$$

where the two body matrix element is evaluated by an obvious change of notation in equation (B.9) except that the factor 0.46 is replaced by 1.0.

4) The matrix element (A, VB):

$$\langle A | V_{nn} | B \rangle = \langle A | V_{pp} | B \rangle = 0. \qquad \text{(B.12)}$$

$$\langle A | V_{np} | B \rangle = (-1)^{J_0 + j_{pp} + j_{pn}} \frac{V_0 F^{J^\pi; pp, pn, hn}}{2 \hat{J}_0}$$

$$\hat{j}_{hn} \hat{j}_{pn} \hat{j}_{pp} \left(- \left[1 + \frac{(1+P)}{2} (-1)^{l_{pn} + l_{hn} + J_0} \right] \right.$$

$$(j_{pn}\ 1/2\ j_{hn}\ -1/2\ |\ J_0\ 0)(j_{pp}\ 1/2\ J\ -1/2\ |\ J_0\ 0) - \frac{(1-p)}{2}$$

$$(-1)^{L_J + l_{pn} + j_{hn} + J + J_0}(j_{pn}\ 1/2\ j_{hn}\ 1/2\ |J_0\ 1)$$

$$(j_{pp}\ 1/2\ J\ 1/2\ |\ J_0\ 1)\Big), \qquad \text{(B.13)}$$

where L_J is the orbital angular momentum associated with J.

5) The matrix element (A, VC):

$$\langle A|V_{nn}|C\rangle = \langle A|V_{np}|C\rangle = 0 \qquad \text{(B.14)}$$

$$\langle A|V_{pp}|C\rangle = \frac{-0.46V_0 F^{J^\pi; pp, pp', hp}}{2\hat{J}_0\sqrt{1+\delta_{pp,pp'}}}\ \hat{j}_{hp}\hat{j}_{pp'}\hat{j}_{pp}$$

$$(-1)^{j_{pp}+j_{hp}+l_{hp}+l_{pp}+1}\left(1+(-1)^{l_{pp}+l_{pp'}+J_0}\right)$$

$$(j_{hp}\ 1/2\ J\ -1/2\ |\ J_0\ 0)(j_{pp}\ 1/2\ j_{pp'}\ -1/2\ |\ J_0\ 0)$$

$$\left[1-(1-P)\left(\frac{1+(-1)^{l_{hp}+L_J+J_0}}{2}\right)\right]. \qquad \text{(B.15)}$$

These expressions were programmed in FORTRAN IV. Computation was done on the TUCC IBM 360-75 computer. The subprograms for the vector coupling coefficients, 6 - j, and 9 - j symbols, as well as the diagonalization routine, were written by R. S. Caswell.

LIST OF REFERENCES

LIST OF REFERENCES

I. R. Afnan, Phys. Rev. 163, 1016 (1967).

E. H. Auerbach, Brookhaven National Laboratory, unpublished report BNL 6562 (1962).

P. M. Beard, "A High Resolution Study of the $^{18}O(p,n)^{18}F$ Reaction," unpublished Ph. D. dissertation, Duke University (1964).

W. P. Beres and M. Divadeenam, in publication, Nucl. Physics, (1968).

W. P. Beres and M. Divadeenam, Physical Review Letters 20, 938 (1968).

W. P. Beres and W. M. MacDonald, Nucl. Physics A91, 529 (1967).

L. C. Biedenharn, J. M. Blatt and M. E. Rose, Revs. Mod. Phys. 24, 249 (1952).

J. M. Blair and J. J. Leigh, Phys. Rev. 118, 495 (1960).

J. M. Blatt and L. C. Biedenharn, Revs. Mod. Phys. 24, 258 (1952).

B. Block and H. Feshbach, Ann. Phys. 23, 47 (1963).

R. R. Carlson, C. C. Kim, J. A. Jacobs and A. C. L. Barnard, Phys. Rev. 122, 607 (1961).

S. Cohen, R. D. Lawson, M. H. MacFarlane and M. Soga, Physics Letters 9, 180 (1964).

A. R. Edmonds, Angular Momentum in Quantum Mechanics, (Princeton University Press, Princeton, New Jersey, 1957).

H. A. Hill and J. M. Blair, Phys. Rev. 104, 198 (1956).

G. A. Keyworth, "A High Resolution Study of Isobaric Analogue States in ^{41}K and ^{23}Na", unpublished Ph. D. dissertation, Duke University (1968). The ^{23}Na results are in publication, Phys. Rev.

G. A. Keyworth, C. G. Kyker, Jr., E. G. Bilpuch and H. W. Newson, Nucl. Physics 89, 590 (1966).

A. M. Lane and R. G. Thomas, Revs. Mod. Phys. 30, 257 (1958).

R. A. Laubenstein and M. J. W. Laubenstein, Phys. Rev. 84, 18 (1951).

T. Lauritsen and F. Ajzenberg-Selove, Energy Levels of Light Nuclei (National Academy of Sciences - National Research Council, Washington, D. C., 1962). Previously published in Nucl. Physics 11, 1 (1959).

H. Mark and C. Goodman, Phys. Rev. 101, 768 (1956).

M. G. Mayer and J. H. D. Jensen, Elementary Theory of Nuclear Shell Structure (Wiley, New York, 1955).

R. Moreh, Nucl. Physics 70, 293 (1965).

P. B. Parks, P. M. Beard, E. G. Bilpuch and H. W. Newson, Rev. Sci. Instr. 35, 549 (1964).

P. B. Parks, H. W. Newson and R. M. Williamson, Rev. Sci. Instr. 29, 834 (1958).

F. W. Prosser, Jr., G. U. Din and D. D. Tolbert, Phys. Rev. 157, 779 (1967).

F. T. Seibel, N. R. Roberson, E. G. Bilpuch and H. W. Newson, Nuclear Instruments and Methods 47, 244 (1967).

E. P. Wigner and L. Eisenbud, Phys. Rev. 72, 29 (1947).

J. L. Wiza and R. Middleton, Phys. Rev. 143, 676 (1966).

K. Yagi, K. Katori, H. Ohnuma, Y. Hashimotto and Y. Nogami, J. Phys. Soc. Japan 17, 595 (1962).

K. Yagi, J. Phys. Soc. Japan 17, 604 (1962).

BIOGRAPHY

David Lee Sellin

Personal: Born 28 March 1941, Milwaukee, Wisconsin.
Married 20 June 1962.

Education: B. S. in Physics, California Institute of Technology, 1962.

Positions: Teaching Assistant, Duke University, 1962-1963.
Research Assistant, Duke University, 1963-1964.
NASA Fellowship, Duke University, 1964-1966.
Research Assistant, Duke University, 1966-present.

Membership: American Physical Society

Publication: ^{40}A(d,p) Excitation Functions over the Ground-State Isobaric Analog Energy Region (with P. Wilhjelm, G. A. Keyworth, G. C. Kyker, Jr., N. R. Roberson, E. G. Bilpuch) Physical Review Letters 18, 130 (1967).

Abstracts:

1. Keyworth, Kyker, Bilpuch, Sellin and Newson, Fine Structure of Isobaric Analogue Resonances in ^{41}K, Bull. Am. Phys. Soc. 11, 82 (1966).

2. Kyker, Keyworth, Sellin, Newson and Bilpuch, ^{40}A + p Scattering and Reaction Cross Sections from 2.6 to 3.2 MeV, Bull. Am. Phys. Soc. 12, 585 (1967).

3. Sellin, Beres, Bilpuch and Newson, States in ^{19}F, Bull. Am. Phys. Soc. 13, 651 (1968).